Master in Chemical Engineering

Development of a new multilayer system for a firefighter's jacket – Preliminary study

Master dissertation

of

Margarida Tavares da Silva

Developed within the course of the dissertation

held in

CeNTI - Centro de Nanotecnologia e Materiais Técnicos, Funcionais e Inteligentes

Supervisor at FEUP: **Dr. Soraia F. Neves**

Joint supervisor at FEUP: **Prof. João Moreira de Campos**

Coordinator at CeNTI: **Eng. João Ribeiro**

July 2021

Acknowledgment

The space dedicated to this section is certainly not enough to thank all the people who, directly or indirectly, contributed to the elaboration of this dissertation. To all of you, my sincere acknowledgment.

First of all, I would like to thank CeNTI for the opportunity to integrate this project and all the resources provided for the accomplishment of my dissertation.

I would also like to acknowledge the FCT - Fundação para a Ciência e a Tecnologia for supporting the DIF-Jacket (ref. PCIF/SSO/0106/2018) project in which my dissertation is inserted.

My sincere acknowledgment to my supervisor at CeNTI, Eng. João Ribeiro, for the support and guidance throughout this dissertation. I also acknowledge my supervisor at FEUP, Dr. Soraia F. Neves, and my joint supervisor at FEUP, Prof. João Moreira de Campos, for all the willingness shown and encouragement given.

I thank all the CeNTI collaborators I had the opportunity to work with, especially Francisca Marques, Eduardo Oliveira and Patrícia Fernandes for all the help, knowledge and accompaniment.

I am grateful to my fellow trainees at CeNTI, especially Joana Kuski, Inês Vilaverde, Mariana Veloso and Kseniia Shevchenko, for all the companionship and for always being available to help me.

Finally, I thank all my family and friends for all their support and words of encouragement.

Abstract

The growth in size and duration of wildland fires in recent years and the increasingly demand for high-performance protective clothing, has led Thermal Protective Clothing Research and Development (TPC) to seek solutions to minimise firefighter thermal load and skin burns. In this context, the present dissertation was developed under the framework of the DIF-Jacket project (PCIF/SSO/0106/2018), with the main goal being the development of a new multilayer system to be used in a jacket of wildland firefighters and the subsequent development of an experimental procedure to evaluate its transient behaviour.

The developed multilayer system consists of three layers: an outer shell, a PCM pouch and an inner layer. Firstly, two outer shells and three inner layers were selected and characterized. Further, the effect of the application of IR reflectors on the outer layer of the multilayer system was studied. Furthermore, the impact of the incorporation of PCMs pouches on the thermal performance of the multilayer system was also analysed. Hence, three different PCMs (two in pure state and one macroencapsulated in silica) and two different pouch construction methods (manual and by bonding) were studied. The mechanical properties of the pouches material were also tested to verify the effect of high-temperature variations. Lastly, an experimental procedure was developed and optimised to evaluate the transient behaviour of the solution under study, simulating the different phases to which a firefighter is exposed to (i.e., direct exposure to a radiative heat flux followed by a post-fire period).

In summary, the application of IR reflectors on the outer shell does not significantly impact the heating delay and, in addition, as a drawback it significantly increases the evaporative resistance of the multilayer system. Regarding the pouch construction, both methods proved to be adequate for the final application. Further, the best temperature homogeneity of the PCM pouches was obtained when the PCM used is macroencapsulated in silica. Lastly, the incorporation of PCMs in the multilayer system significantly delays its heating. However, it also significantly delays its cooling and increases its weight and evaporative resistance.

Keywords: Multilayer system, heat transfer, IR reflectors, PCMs, PCM pouch, transient behaviour

Resumo

O aumento do tamanho e da duração dos incêndios florestais nos últimos anos e a crescente procura por vestuário de proteção para bombeiros com alto desempenho levou a Investigação e Desenvolvimento de Vestuário de Proteção Térmica (TPC) a procurar soluções para minimizar a carga térmica do bombeiro e as respetivas queimaduras cutâneas. Neste contexto, a presente dissertação foi desenvolvida no âmbito do projeto DIF-Jacket (PCIF/SSO/0106/2018), tendo como principal objetivo o desenvolvimento de um novo sistema multicamada para um casaco de bombeiros florestais e o posterior desenvolvimento de um procedimento experimental para avaliar o seu comportamento transiente.

O sistema multicamada desenvolvido consiste em três camadas: uma camada têxtil exterior, uma bolsa de PCM e uma camada têxtil interior. Em primeiro lugar, seccionaram-se e caracterizaram-se duas camadas têxteis exteriores e três interiores. Além disso, estudou-se o efeito da aplicação de refletores IV na camada exterior do sistema multicamada. Adicionalmente, estudou-se o impacto da incorporação de bolsas de PCMs no desempenho térmico do sistema multicamada. Assim, estudaram-se três PCMs diferentes (dois em estado puro e um macroencapsulado em sílica) e dois métodos diferentes de construção de bolsas (manual e por união). As propriedades mecânicas do material das bolsas foram também testadas para verificar o efeito de variações elevadas de temperatura. Por fim, desenvolveu-se e otimizou-se um procedimento experimental para avaliar o comportamento transiente da solução em estudo, simulando as diferentes fases a que um bombeiro está exposto (ou seja, exposição direta a um fluxo de calor radiativo seguido de um período pós-incêndio).

Em resumo, a aplicação de refletores IV na camada exterior não tem um impacto significativo no atraso do aquecimento e, além do mais, tem como desvantagem aumentar significativamente a resistência evaporativa do sistema multicamada. Relativamente à construção da bolsa, ambos os métodos mostraram ser adequados para a aplicação final. Para além disso, a distribuição de temperatura mais homogénea foi obtida com o PCM macroencapsulado em sílica. Por fim, concluiu-se que a incorporação de PCMs no sistema multicamada atrasa significativamente o seu aquecimento. Contudo, também atrasa significativamente o seu arrefecimento e aumenta o seu peso e resistência evaporativa.

Palavras-chave: Sistema multicamada, transferência de calor, refletores IV, PCMs, bolsa com PCM, comportamento transiente

Declaration

I hereby declare, under word of honour, that this work is original and that all non-original contributions is indicated and due reference is given to the author and source

July 5th, 2021

Margarida Tavares da Silva

(Margarida Tavares da Silva)

Index

List of Figures

List of Tables

Notation and Glossary

A	Area	m^2
c_p	Specific heat	$kJ \cdot kg^{-1} \cdot ºC^{-1}$
dm/dt	Evaporation rate of moisture leaving the foot manikin's surface	$kg \cdot s^{-1}$
H_c	Heating power supplied to the foot manikin	W
I	Index	
I_t	Thermal insulation	$m^2 \cdot ºC \cdot W^{-1}$
k	Thermal conductivity	$W \cdot m^{-1} \cdot ºC^{-1}$
L	Thickness	mm
P	Water vapour pressure	kPa
R	Reflectance	%
R_e	Evaporative resistance	$kPa \cdot m^2 \cdot W^{-1}$
RH	Relative humidity	%
t	Time	s
T	Temperature	ºC

Greek Letters

ε	Emissivity	
λ	Water vaporisation enthalpy	$J \cdot kg^{-1}$
$\Delta C'$	Chroma difference	
ΔE_{2000}	Colour difference	
ΔH	Latent heat	$kJ \cdot kg^{-1}$
$\Delta L'$	Lightness difference	

Indexes

a	ambient
air	Air within the climatic chamber
c	Copper sample
m	Melting
max	Maximum operating
mp	Moisture permeability
s	Surface of the foot manikin

List of Acronyms

ASTM	American Society for Testing and Materials
CEFT	Centro de Estudos de Fenómenos de Transporte
CEIIA	Centro de Excelência para a Inovação da Indústria Automóvel
CeNTI	Centro de Nanotecnologia e Materiais Técnicos, Funcionais e Inteligentes
CITEVE	Centro Tecnológico das Indústrias Têxtil e do Vestuário de Portugal
CTIC	Centro Tecnológico das Indústrias do Couro
EN	European Standard
FR	Flame Retardant
IR	Infrared
ISO	International Organization for Standardization
LOI	Limiting Oxygen Index
NIR	Near infrared
PCM	Phase Change Material
SMA	Shape Memory Alloy
T1	Data logger 1
T2	Data logger 1
T3	Data logger 1
TES	Thermal Energy Storage
TPC	Thermal Protective Clothing
UV	Ultraviolet
Vis	Visible
XPS	Extruded Polystyrene

1 Introduction

1.1 Framing and presentation of the work

A substantial expansion of the fire-prone area and longer fire seasons are expected due to climate change in most regions of Europe, especially in Portugal that has one of the highest forest fire risk ratings [1, 2]. This growth in wildfires and, consequently, the stronger need for high-performance protective clothing by firefighters has led Thermal Protective Clothing (TPC) Research and Development to search for solutions to minimize firefighter's heat load and skin burns.

To contribute to the advance of knowledge in the TPC field, the project DIF-Jacket ((PCIF/SSO/0106/2018) combines the available solutions and techniques to produce Thermal Protective Clothing with outstanding performance. The project joins together the three different institutions: CeNTI - Centro de Nanotecnologia e Materiais Técnicos, Funcionais e Inteligentes, CITEVE – Centro Tecnológico das Indústrias Têxtil e do Vestuário de Portugal and CEFT - Centro de Estudos de Fenómenos de Transporte, and its main goal is to produce an innovative thermal protective jacket for firefighters [3].

Promising numerical results were already obtained showing the potential of phase change materials (PCMs) to increase the thermal protection of firefighter's bodies during the different phases of firefighting [4]. For that reason, the next step is to develop a new solution following the multilayer system of a convectional jacket structure with the addition of PCMs incorporated through pouches. Furthermore, it is also intended to develop an experimental procedure for evaluating the transient behaviour of the multilayer system, to simulate the different phases of firefighting to which the firefighter is exposed to.

1.2 Presentation of the company

CeNTI - Centro de Nanotecnologia e Materiais Técnicos, Funcionais e Inteligentes is a private non-profit R&D institute located in Vila Nova de Famalicão and its mission is to develop and validate new technologies based on the development of new smart and functional materials and systems. CeNTI is the result of a strong collaboration between CITEVE – Centro Tecnológico das Indústrias Têxtil e do Vestuário de Portugal, University of Porto, University of Minho, University of Aveiro, CTIC - Centro Tecnológico das Indústrias do Couro and CEIIA - Centro de Excelência para a Inovação da Indústria Automóvel, all recognised nationally and internationally for their technological innovation. Founded in 2006, CeNTI has 15 years of activity, 67 active patent applications and over 170 projects with industries such as textile, chemical and automotive.

1.3 Contribution of the author to the work

In the scope of this dissertation, I developed an innovative multilayer system with integrated PCMs for firefighter jackets. I also developed an experimental procedure to evaluate the transient behaviour of the multilayer system, which I optimized the set-up, to simulate the different phases of firefighting to which a firefighter is subject to (i.e., direct exposure to a radiative heat flux followed by a post-fire period). Besides the incorporation effect of PCMs, I also studied the impact of the application of IR reflectors on the thermal performance of the multilayer system. Furthermore, I characterized the thermal and evaporative properties of the fabrics and the pouches material's mechanical properties.

1.4 Organization of the dissertation

The dissertation is divided into six chapters and contains ten appendices. The first chapter is the introduction, which includes a framework of the work carried out and the author's contribution, as well as the presentation of the company and the organization of the dissertation. The second chapter contains the context and state of the art of the firefighter protective clothing and its conventional structure (as multilayer system), and the analyses of the latest functional materials that can be used to improve the clothing thermal performance. In the third chapter, the materials studied and the methods and equipment used in the development of the multilayer system are described. Chapter four shows the main results obtained and discussed, and the main conclusions are presented in the fifth chapter. The sixth and final chapter contains the work's evaluation, which involves the objectives achieved, limitations and future work, and a final evaluation.

2 Context and State of the art

2.1 Firefighter's Protective Clothing

The firefighter's protective clothing has undergone significant improvements in recent decades. The introduction of high-performance fibers (e.g., Nomex®) in the 1960s completely changed and improved the level of protection, marking the end of the rubber protective clothing worn by previous generations of firefighters [1]. However, the protective gear was bulky and heavy because all the dress layers were made of Nomex®, which was almost twice as heavy as it is today [2]. Nowadays, the firefighter's protective clothing can be classified according to its purpose: Structural and Proximity Firefighting Protective Clothing regulated by EN 469 or Wildland Protective Clothing regulated by ISO 15384. Structural fires are characterised by high heat fluxes and short exposure times (i.e., seconds to minutes of exposure) and the protective clothing designed for this type of hazard consists of three layers which provide high thermal protection: an outer shell, a moisture barrier and a thermal barrier [5]. By comparison, wildland fires are characterised by lower heat fluxes and longer exposure times (i.e., hours), as well as higher physical activity. For that reason, wildland firefighters are also exposed to high heat loads. Besides protection against heat from the fire, the protective clothing must ensure that the high levels of internal metabolic heat produced during intense exercise are eliminated to the ambient to prevent heat stress injuries. Thus, a protective equipment with three layers like the Structural and Proximity Firefighting Protective Clothing would not be suitable [6]. For that reason, Wildland Protective Clothing is lighter and consists of only one layer, usually with the same materials as an outer shell of Structural and Proximity Firefighting Protective Clothing [6].

Until recently, firefighter's protective clothing was focused on maximum thermal protection and was designed and developed following evaluation methodologies mainly in steady-state (e.g., thermal insulation and evaporative resistance [7, 8]) or under short-term transient conditions (e.g., protection against radiant heat [9]). Currently, beyond the high thermal performance, the protective clothing is also expected to facilitate the firefighter metabolic heat and sweat vapour transfer to the environment, improving thermal comfort performance [10]. Unfortunately, there are few studies where protective clothing design is optimized based on this set of scenarios and the methodologies described in the literature do not evaluate of the protective clothing heating/cooling cycles. Thus, this dissertation aims to develop a new multilayer system with integrated PCMs, taking into account its transient behaviour. This evaluation is fundamental and a new methodology for evaluating the protective clothing under transient conditions must be created [4].

Thermal protection and thermophysiological comfort of firefighter's protective clothing is determined by the heat and mass balance between the human body and the environment, which is clearly related to the properties of the fibers and layers of the protective clothing [11]. Therefore, it is crucial to understand all the phenomena involved and the main properties of firefighting protective clothing to obtain an upgraded product in terms of heat protection and comfort.

2.1.1 Main phenomena

At the external boundary of firefighter's protective clothing exposed to the environment, heat transfer from the outside to the inside of firefighter's protective clothing can occur by conduction, convection and radiation or by a combination of these mechanisms. Heat transfer by conduction occurs when there is contact with hot surfaces or melted substances and is less common in firefighting [12]. Heat transfer by convection with surrounding hot gas (air and smoke) and by radiation emitted from the flames are the most common heat transfer mechanisms and are major hazards for firefighters [13]. In addition, the firefighter's body generates metabolic heat (at the boundary near the skin), which is transferred to the protective clothing, either by conduction (no gaps between the skin and the protective clothing), natural or forced convection, and/or radiation (emitted by the human body) [10].

When the human body feels the need to cool down during firefighting, besides releasing metabolic heat, it also releases sweat. As sweat is produced, it accumulates near the skin and gradually evaporates (partially). If the rate of evaporation is significantly lower than the rate of sweat production, there will be a considerable accumulation of sweat near the skin, increasing discomfort and increasing the risk of friction burns [11].

2.1.2 Properties

In general, the main thermal protection property of clothing is thermal insulation, which considers the three heat transfer mechanisms: conduction, convection and radiation [7]. To reduce the heat transfer by conduction from the environment to inside the clothing, one solution would be to increase the thickness and density of the firefighter's protective equipment [12]. This solution is not ideal due to the increase in weight and consequent difficulty in moving around and increased metabolic activity. The preferred option is to use materials with low thermal conductivity [14]. To minimize convective heat transfer, firefighter's protective clothing should have low air permeability [15]. Although the moisture transport through the air allows a quick release of metabolic heat which favours thermal comfort, a high air permeability implies a reduction of thermal insulation and a worse thermal performance [16]. Lastly, the effect of radiative heat transfer can be reduced by increasing the reflectance or decreasing the emissivity of the materials [12].

Regarding the mass transfer occurring in firefighter's protective clothing, the property to be considered is evaporative resistance. Evaporative resistance is the resistance to the flow of water vapour from the wearer's body to the environment provided by the fabric. The smaller it is, the lower the chance of heat stress [4].

The moisture permeability index is an important parameter in clothing characterisation that expresses the relationship between thermal insulation and evaporative resistance. The moisture permeability index is commonly used to determine the degree of evaporative cooling (i.e., how quickly the sweat is evaporated through the clothing), and it is calculated by equation (1):

$$I_{\mathrm{mp}} = K \times \frac{I_t}{R_e} \tag{1}$$

where I_{mp} is the moisture permeability index (dimensionless), K a constant with value 60.65 $Pa \cdot {}^{o}C^{-1}$, I_t the thermal insulation in $m^2 \cdot {}^{o}C \cdot W^{-1}$ and R_e the evaporative resistance in $Pa \cdot m^2 \cdot W^{-1}$ [17].

2.2 Multilayer Structure of Firefighter's Protective Clothing

Protective clothing for firefighters is essential not only to provide thermal protection, but also to ensure an adequate level of comfort in situations of extreme firefighting conditions. To achieve these properties, the clothing worn by firefighters consists of a multilayer system with three main layers: outer shell, moisture barrier and thermal liner [16]. This multilayer system is shown in Figure 1.

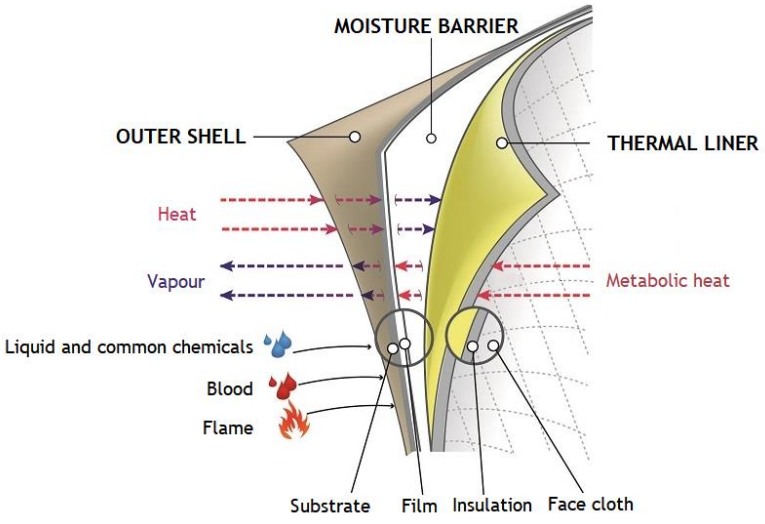

Figure 1 - Multilayer structure of firefighter's protective clothing (adapted) [18].

2.2.1 Outer Shell

The outer shell is the most external fabric of the firefighter's protective clothing and the first line of defence for firefighters. Its principal function is to protect the firefighter against direct flame and must have sufficient tensile strength with acceptable abrasion and cut resistance to withstand crawling or climbing if required [16].

Commercially, a blend of two or more inherently high-performance flame retardant fibers is commonly used so that a balance can be reached between cost, protection and comfort. The most widely used fibers in outer shells of firefighters' protective clothing are:

- **Nomex®** - is the most widely used m-aramid and is known for its good thermal tolerance and long-term stability at high temperatures [1]. In addition to high UV resistance, this fiber offers excellent thermal insulation through thermal energy absorption when exposed to heat [19].
- **Kevlar®** - is the most well-known p-aramid and is used because of its high tensile strength and cut resistance. Although this fiber has good heat resistance, it hardly absorbs heat energy when exposed to heat, so most of the energy passes through the fabric [19].
- **PBI®** - has excellent thermal protection and flame-resistant properties and is stable at high temperatures. However, PBI® has relatively low tensile strength, low UV resistance and degrades rapidly in humid environments. Given its high cost, it is usually blended with aramid fibers to optimise the cost-performance ratio [10, 14]. This type of fiber can easily withstand temperatures of 600 ºC for a short period of time and 300-350 ºC for longer exposure times [10].
- **PBO** - is a liquid crystalline polybenzoxazole with significantly high heat and flame resistance. This fiber has high tensile strength and it is around 1.6 times stronger than Kevlar® and 10 times stronger than PBI® fiber [16]. PBO has a very high thermal stability due to its symmetrical linear repeating aromatic chemical structure, with a decomposition temperature of 650 ºC. However, it is a heavy and high-cost fiber and it is usually blend with aramid fibers or PBI® [10].

2.2.2 Moisture Barrier

The moisture barrier makes a firefighter's protective garment impermeable to water, blood pathogens and common liquid chemicals, while it allows water vapour, which is metabolically produced by the human body, to pass through. Therefore, the firefighter is protected against water and substances that may be toxic and thermal comfort is improved by allowing perspiration to dissipate into the environment [16].

The moisture barrier is placed between the outer shell and the thermal liner and, generally, consists of two components: film and substrate (as shown in Figure 1). The film consists of a microporous polymeric membrane, usually ePTFE, which does not allow water and other liquids to pass through but is permeable to water vapour. The membrane can also be laminated or coated with another material such as polyvinyl chloride, polyurethane or polyester. The substrate is a woven or non-woven fabric with flame retardant fibers, laminated together with the film component to support it [4, 14].

2.2.3 Thermal Liner

The thermal liner is the inner layer and the most important component in a firefighter's protective equipment, since it provides the majority of thermal protection and significantly reduces heat stress [16].

Two elements are usually required to assemble a thermal liner: a batting fabric and a face cloth. Both are manufactured using flame retardant fibers. However, the batting fabric is a felt/non-woven fabric, while the facing fabric is a woven/spun-laced nonwoven fabric [10].

2.3 Functional Materials for Improving Thermal Performance

The intense demands of the protective clothing market and the technological development in the textile industry encourage the development of protective clothing with high thermal protection while maintaining high comfort performance [10, 14]. The incorporation of functional materials such as flame retardants (FRs), IR reflectors, phase change materials (PCMs) and shape memory alloys (SMAs) bring benefits. They increase ignition temperature, reflectance and thermal insulation of the materials, resulting in a more significant impediment to heat transfer and possibly a longer exposure time to fire.

2.3.1 Flame Retardants (FRs)

Most fibers, whether natural or synthetic, can easily ignite in the presence of oxygen and high temperatures, resulting in the release of gaseous substances, water vapour and radiant heat, which is a major threat to safety and health of the firefighter. Since the main component of a garment is the fibers, it is of utmost importance to improve the flame retardancy of textile fibers to produce protective clothing with high thermal performance [10].

A flame retardant (FR) is used to slow down the decomposition and increase the ignition temperature of materials, making them more difficult to ignite [20]. For a fiber to be considered flame resistant, it needs to have a limiting oxygen index (LOI) greater than 21 %, which means that more than 21 % of oxygen is required for the fiber to withstand combustion after ignition. Flame retardant fibers can be classified into two groups: chemically modified flame retardant fibers and inherently flame retardant fibers [4, 10].

Chemically modified flame retardant fibers can be produced by various techniques, depending on whether the fibers are natural (e.g., wool, cotton and viscose) or synthetic (e.g., polyester, nylon and acrylic). Flame retardant materials (halogen, nitrogen, silicon and phosphorus) can be applied to a specific fiber as an additive or a finishing agent. In synthetic fibers, flame retardant materials can be incorporated during the polymerisation process (melt spinning) or doped into the spinning bath during fiber production (solution spinning). In addition, both natural and synthetic fibers can be finished by flame retardant materials to convert them into chemically modified flame retardant fibers [4, 10]. Some examples of chemically modified flame retardant fibers are FR cotton, FR viscose, FR vinylon and FR polyester [21].

Regarding inherently flame retardant fibers, the addition of flame-retardant materials as an additive or finishing agent is not required because the flame-resistant properties are intrinsic to the polymer or fiber structure. The presence of aromatic groups in the chemical structure and the high C-C and C-N dissociation energies give high thermal stability to the fibers, resulting in high decomposition and melting temperatures [9, 10]. The most commonly used inherently flame retardant fibers are polyamide (Kevlar® and Nomex®), polyimide fiber (P84®), polybenzimidazole (PBI®), polyamide-imide (Kermel®) and polybenzoxazole (PBO) [4, 16].

Although flame retardant fibers are widely used in protective clothing, they have some drawbacks such as the poor handle and dyeability of high temperature resistant fibers, the low mechanical strength of FR cotton and FR viscose fibers and the melt-drip characteristic of thermoplastic FR fibers. However, blending these fibers with others shadows some of their disadvantages, resulting in a fabric with good thermal and mechanical performances [21].

2.3.2 IR Reflectors

Heat transfer by radiation represents one of the greatest threats to the health and well-being of the firefighter. As already seen in section 2.1.2, one of the approaches to minimise radiant heat transfer is the use of materials with high reflectance. Since the radiation emitted by the fire is equivalent to infrared electromagnetic radiation, the use of IR reflectors can increase the thermal protection performance of protective equipment, by increasing the energy emitted by the clothing surface and so reducing the heat gain [23].

Composite fabrics have been developed, in which the surface is laminated with aluminised films, reducing, in this way, the amount of radiant heat transferred through firefighter's protective equipment during firefighting. Shanghai C&G Safety Co., Ltd is a specialized personal protective clothing company with a range of aluminized protective clothing available [24]. This type of fabric is mainly used to protect against high levels of radiant heat (e.g.,

high proximity firefighting or fires in chemical industries) and it can reflect between about 80-90 % of infrared radiation, whereas most fabrics without this reflectance capability only reflect about 10 %. Thus, incorporating IR reflectors in protective clothing can increase the time that the firefighter can be exposed to fire with no harm [25].

2.3.3 Phase Change Materials (PCMs)

The thermal performance of protective clothing can potentially be improved by increasing the thermal energy storage capacity [16]. Thermal energy storage (TES) is one of the key technologies for the use of thermal energy, in which temporary storage of heat or cold occurs for later use [17, 21]. Among the different alternatives for thermal energy storage (i.e., sensible heat utilization, reversible chemical heat utilization and heat of dilution utilization), latent heat storage is particularly attractive since it not only allows better thermal storage using much lower mass (high storage density), but it also allows an efficient usage, as the energy is stored at nearly isothermal conditions [26].

Phase change materials (PCMs) are materials that can be used to absorb/release energy in the form of latent heat through a phase transition [22, 23]. The most used phase transition in commercial applications is solid-liquid due to its relatively large energy storage with acceptable volume variation (≤ 10 %) over a small temperature range [19]. The PCM needs to be encapsulated or contained somehow so that the PCM doesn't leak when in the liquid state [29]. Phase transitions involving gas have very large transition enthalpies, but are not usually used because expensive and possibly dangerous pressure vessels are required to contain a large mass of gas [30].

Incorporating PCMs into firefighter's protective clothing can be used to absorb metabolic heat produced by the human body (enhancing comfort), or to absorb heat from the environment (enhancing protection). When incorporated into the firefighter's protective clothing, PCMs can absorb the heat metabolically produced by the human body during its melting process, giving the wearer a cooling effect [31]. Within the scope of this dissertation, PCMs will be incorporated into the firefighter's protective jacket to absorb the heat from the fire to increase the time that the firefighter can be exposed to it. However, it is also crucial to release the energy accumulated during fire exposure, as excessive heat accumulation promotes the occurrence of third-degree burns, limiting the time the firefighter has to remove the garment [32]. Recent studies found that the optimum position for the PCM layer is the closest to the external heat source since it favours a higher use of the PCM storage capacity and takes advantage of its high thermal inertia in a more efficient way [33]. Figure 2 shows a schematic representation of the solid-liquid phase change process.

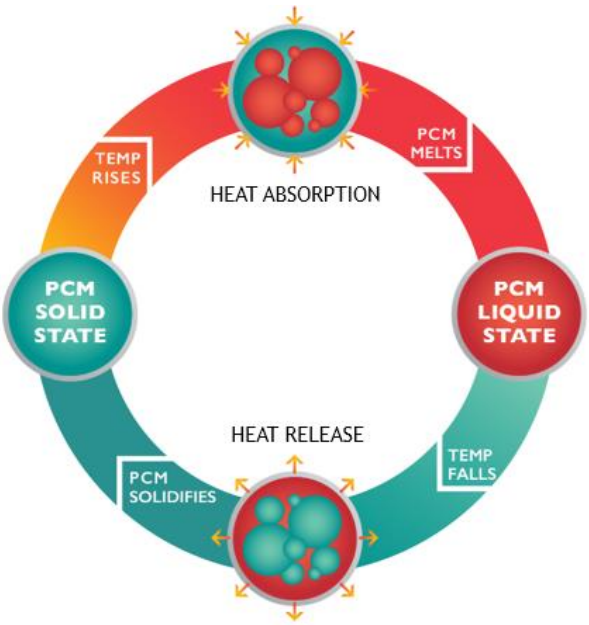

Figure 2 - Schematic representation of solid-liquid phase change process (adapted) [34].

The wide range of PCMs available on the market is grouped into two main categories: organics and inorganics [33]. Organic PCMs (e.g., paraffins, linear alkyl hydrocarbon and polyethylene glycols) have a large latent heat capacity and are available in a wide range of temperatures. This type of PCMs tends to be chemically stable and maintain effectiveness after many thermal cycles, but typically has low thermal conductivity and low discharging rates. Inorganic PCMs (e.g., hydrated inorganic salts, eutectics and polyhydric alcohol-water solution) have high latent heat storage capacity storage and a large melting point range, with a lower cost than organics. However, this type of PCMs can experience loss of effectiveness with thermal cycling, a large degree of super cooling, it is corrosive and it cannot be microencapsulated [16, 31].

RUBITHERM® is one of the main PCM suppliers worldwide. They provide inorganic and organic PCMs in large and small quantities and offers solutions in a wide temperature range from about -10 ºC to 90 ºC [34]. PLUSS® is a materials research and manufacturing company in and have a wide variety of PCMs available for various applications with a melting temperature range from -33 ºC to 89 ºC [35]. With more sustainable solutions, CRODA is a UK-based company that manufactures bio-based phase change materials under the trade name CrodaTherm™. The PCMs produced are organic and plant-derived and available in temperatures between 5 ºC and 74 ºC [36].

A determining factor in selecting the most suitable PCM for a specific application is the melting temperature [29]. When the purpose of incorporating PCMs in a garment is protection by absorbing heat from the environment, the melting temperature should be high enough so that the melting of the PCM does not start before the exposure (e.g., due to human body

metabolic heat), but it also should be low enough to ensure that the PCM melts fully in any exposure scenario at its maximum possible efficiency. Another consideration when choosing the PCM is the latent heat. Generally, it is recommended to select a product with high latent heat to store a large part of the incoming energy [28].

PCMs are highly versatile materials, which can be incorporated into protective clothing in a variety of ways. Microencapsulation is an efficient way of containing PCMs and one of the most widely used. This method involves creating a microscopic container around the PCM and allows it to be incorporated into a wide range of materials using different techniques according to the intended application. Coating, lamination, finishing, bi-component synthetic fiber extrusion, and foam techniques are some of the processes used to incorporate PCMs into the textile matrix. Macroencapsulation is another alternative for containing PCMs, which involves incorporating PCMs into some container like a pouch, plastic container, piping, panels or bulk container [17, 24]. Studies have shown that the use of microencapsulated PCMs, coating and lamination in garments has a very low capacity to receive excess heat and is insufficient to ensure improved thermal comfort in a hot working environment. On the other hand, textile products, in which macroencapsulated PCMs are placed have a higher capacity to receive an excess heat and are, therefore, the most suitable for application in protective clothing against heat [37].

Although the inclusion of a PCM layer in fire protective clothing significantly increases its thermal performance, there are some disadvantages. Among them are the burning behaviour, durability problems, increasing evaporative resistance and clothing weight [18].

2.3.4 Shape Memory Alloys (SMAs)

To improve the ergonomics of protective clothing, it is important that the protective properties vary according to the level of hazard. Therefore, a firefighter's protective equipment should provide adequate thermal insulation only when exposed to heat and offer less thermal insulation concordant with comfort requirements under normal conditions after the end of exposure [13, 15].

Shape memory alloys (SMAs) are smart materials that are usually incorporated between two layers of fabric and that, under the influence of temperature stimuli form an air gap that improves thermal insulation by increasing resistance to heat transfer (Figure 3) [15, 26]. The most popular and useful shape of SMAs is helical coil springs, since this kind of springs can be used either in extension or compression, providing an impressively large stroke and may be designed to exert significant forces [37].

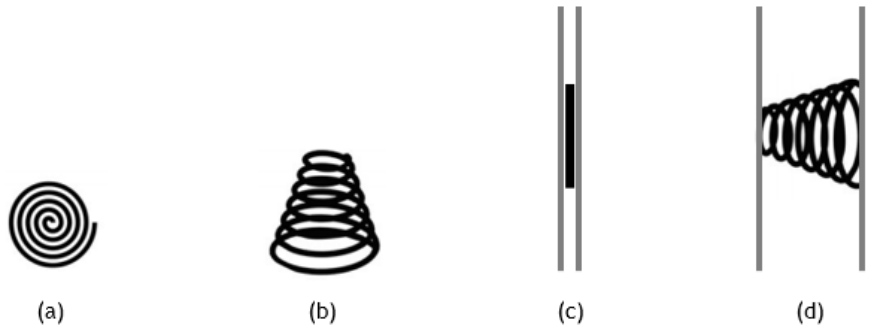

Figure 3 - Schematic representation of: (a) non-actuated spring, (b) actuated spring, (c) non-actuated spring between layers of fabric, and (d) actuated spring between layers of fabric (adapted) [39].

SMAs show changes in its alloy when the environmental temperature is lower or higher than its actuation temperature [40]. When the environmental temperature is lower than the actuating temperature, the alloy exhibits a uniform martensite structure with low yield strength and is easily deformed. However, when the environmental temperature is higher than the actuating temperature, the alloy increases in stiffness and it exerts a given force when returning to a shape previously incurred by the heat treatment [39]. Studies have shown that the actuating temperature of the SMAs should be in a temperature range between 50 and 60 ºC, in order to guarantee that the beginning of shape change of SMAs elements occurs when the outer surface of the textile system reaches 60 ºC, so that the skin temperature does not exceed the pain threshold, which is 44 ºC [19].

The application of SMAs in firefighter's protective clothing brings many advantages, such as increased thermal insulation using much lighter and thinner materials. An important feature of these materials is that they take into account the transient behaviour of the firefighter, as the protective properties of the clothing adapt according to the environmental working conditions [19]. Furthermore, this type of approach is environmentally friendly because it uses air and does not require any external power supply, thus having a longer lifespan than other intelligent textiles using power supplies [40]. However, a major limitation of incorporating SMAs is that protective clothing can easily be compressed in some situations. When the garment is compressed, it restricts the opening capacity of the material and enhances the heat conduction of the metal spring. Hence, there are more drawbacks than benefits. Therefore, it is suggested that the SMA spring should not be placed on the areas of the protective clothing that can be easily compressed such as the elbow, knee and back, but rather on areas that are directly exposed to the heat source, such as the chest and arms [18].

3 Materials and Methods

A multilayer system at a small scale with integrated PCMs was studied to design an innovative firefighter jacket with high thermal performance. The multilayer system consists of three layers tested individually and then as a whole: an outer shell, an intermediate layer with the PCM pouches, and an inner layer. The inner layer was included to support the PCM pouches and prevent them from being in direct contact with the skin.

3.1 Materials

3.1.1 Fabric selection and composition

All the fabrics used are commercial products developed for firefighter's protective equipment and their selection was made according to several criteria. In general, composition is an important parameter. Different compositions allow previewing the influence of different fibers on the protection offered (e.g., p-aramid offers mechanical strength, while m-aramid offers thermal resistance, as seen in section 2.2). In addition, priority was given to fabrics that already have protection certifications. Regarding the fabric for outer shells, the choice of different colours and the amount of sample available were the decisive factors, since these materials will be functionalised with IR reflectors. Lastly, in the selection of the inner layer, two thermal liners (batting fabric + face cloth) and two face cloths of each of the thermal liners were chosen. This choice aims to evaluate the influence of the thickness and composition of the additional layer on thermal performance. The composition of the fabrics under study for the multilayer system is presented in Table 1, and their certifications are in Appendix A.

Table 1 – Composition of the fabrics tested

Fabric	Composition
Outer shell A	P-aramid, m-aramid and static-control
Outer shell B	PPAN-FR, FR rayon, p-aramid and static-control
Inner layer A	Lenzing FR and aramid + Lenzing FR, aramid and polyamide
Inner layer B	M-aramid and p-aramid + Kevlar filament, FR rayon, p-aramid and nylon
Inner layer C	Lenzing FR, aramid and polyamide
Inner layer D	Kevlar filament, FR rayon, p-aramid and nylon

3.1.2 IR reflectors formulation

The outer shells were optimised by applying a formulation with IR reflectors in order to increase the reflectance of their surfaces while trying to have minimal impact on the colour. The components used in the manufacture of the yellow IR reflector formulation are shown in Table 2.

Table 2 – Components used in IR reflectors formulation

Component	Chemical Characterization
IR reflective pigment	Nickel antimony titanium
Binding agent	Styrene acrylic copolymer
Wetting agent	Polyether siloxane copolymer
Anti-foaming agent	Mixture of paraffinic mineral oils and hydrophobic components
Thickening agent	Hydroxyethyl cellulose

3.1.3 PCMs pouches

Three different PCMs were studied to incorporate PCM pouches into the firefighter's protective jacket: A, B and C. The choice of the PCMs was mainly according to the results obtained in previous studies. In addition, their availability in the market, cost and minimum order quantity required by the suppliers were taken into consideration. The PCMs under study were supplied by RUBITHERM® and their main thermophysical properties are presented in Table 3.

Table 3 - PCMs and their thermophysical properties

PCM	Form (at 25 °C)	T_m / °C	ΔH_m / kJ·kg^{-1}	c_p / kJ·kg^{-1}·°C^{-1}	k / W·m^{-1}·°C^{-1}	T_{max} / °C
A	Solid	56-59	220	2	0.6	85
B	Solid	69-73	120	2	0.6	90
C	Solid (powder)	77-85	75	2	0.1	110

In the PCMs pouches construction, a polymer X film with a thickness of 0.075 mm was used. Polymer X is a polyimide film that was chosen due to its high thermal resistance and ability to maintain its excellent mechanical properties under hot severe environmental conditions.

3.2 Methods

3.2.1 Thickness

Fabric thickness can be measured using various methods (e.g., with an apparatus featuring a pressure-foot that exerts a specific pressure on the fabric) with excellent reproducibility. However, the thickness of the fabrics was measured through a digital calliper, as it was the option available in the laboratory.

3.2.2 Weight

To determine the weight of the fabric (i.e., the mass of the fabric per area), the area was determined using a ruler and the mass through an A&D GH-252 analytical balance.

3.2.3 Emissivity

The emissivity of a surface is a measure of its ability to emit energy as thermal radiation compared to a black body and it can be determined by direct measurement using an emissometer according to ASTM C 1371.

The emissometer model used is AE1 (Figure 4), which consists of a differential thermopile that imposes a temperature difference between the equipment and the substrate, and a detector that subsequently detects the radiant heat flux emitted by the substrate. The radiant heat flux is then converted into emissivity values through a readout device. This equipment also contains two reference standards that are used to calibrate the equipment: one consisting of a polished stainless steel standard (emissivity about 0.06) and a blackened standard (emissivity about 0.88). The reference standards are placed on the top of a heat sink and, after thermal equilibrium, calibration (Appendix B) is performed and the emissivity is measured directly on the sample. The emissivity must be measured in multiple areas of the sample, until 6 replicas are obtained, which must not show variations in the peak [41].

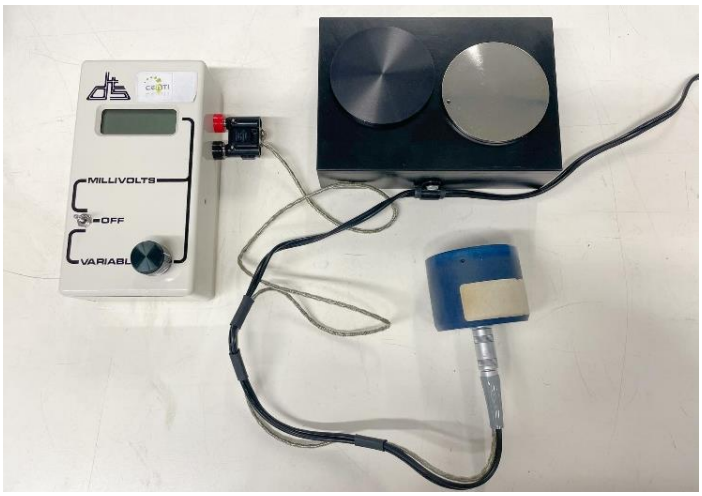

Figure 4 – Emissometer.

3.2.4 Thermal manikin tests

To determine the thermal insulation and the evaporative resistance of fabrics, a thermal foot manikin produced by Measurement Technology Northwest with model 9-zone sweating thermal foot was used. The thermal foot manikin is divided into several zones, each zone having a heating and sweating system. The zone chosen for the study of thermal insulation and evaporative resistance was the heel, since it was the only zone where the whole area could be covered with the fabric sample. The fabrics of the clothing ensemble to be tested were placed on the heel of the foot thermal manikin in the same arrangement as in practical use (i.e., inner side in contact with the manikin skin and outer side exposed to the environment). To support the fabrics, a black sock was used, as shown in Figure 5.

(a) (b)

Figure 5 - Measurement of (a) thermal insulation and (b) evaporative resistance by means of a thermal foot manikin.

These tests were carried out under controlled environmental conditions in an Aralab climatic chamber with model Fitoclima 24000EDTU30. The environmental conditions vary according to the test and they are presented in Table 4.

Table 4 - Environmental conditions during thermal insulation and evaporative resistance tests in the climatic chamber

Test	T_{air} / °C	*RH* / %
Thermal insulation	20.0 ± 5.0	50 ± 5
Evaporative resistance	35.0 ± 0.5	40 ± 5

The thermal insulation was determined based on the standard ISO 15831. This standard establishes that the temperature of the thermal foot manikin should be 34.0 ± 0.2 °C and, as the operating principle is by temperature set point, the thermal foot manikin will release a heat flow to maintain its temperature stable. This heat flow (from the manikin's skin surface area through the clothing into the ambient air) is measured after steady-state conditions are

reached (i.e., when the coefficient of variation of the heat flux is less than 2 %). From this heat flux, it is possible to determine the heating power supplied to the thermal foot manikin, which is used to calculate the thermal insulation of fabrics through equation 2:

$$I_t = \frac{(T_s - T_{air}) \times A}{H_c} \quad (2)$$

where I_t is the total thermal insulation of the fabric and surface air layer in $m^2 \cdot ºC \cdot W^{-1}$, T_s the surface temperature of the thermal foot manikin in ºC, T_{air} the air temperature within the climatic chamber in ºC, A the surface area of the thermal foot manikin segment and H_c the heating power supplied to the thermal foot manikin in W [7].

The evaporative resistance of the fabrics was measured following the standard ASTM F 2370 in isothermal conditions (T_s = T_{air} = 35 ± 0.5 ºC). The thermal manikin foot delivers a controlled rate of water through the pores in each zone throughout the test to mimic the sweat produced by the human body. A "skin" tight-fitting sock was used (in orange in Figure 5 (b)) to ensure an even water distribution along the whole thermal manikin foot. The skin was saturated with water by spraying before the test to ensure that the vapour pressure at the skin's surface is 100 % and the sweating rate in the pores is high enough to saturate the skin [31]. From the water vapour pressure gradient between the skin and environment it is possible to determine the evaporative resistance using equation 3:

$$R_e = \frac{(P_s - P_a) \times A}{\lambda \times \frac{dm}{dt}} \quad (3)$$

where R_e is the total evaporative resistance of the fabric and surface air layer in $Pa \cdot m^2 \cdot W^{-1}$, P_s the water vapour pressure at the manikin's sweating surface in Pa, P_a the water vapour pressure in the air flowing over the fabric in Pa, A the surface area of the thermal foot manikin segment (that is sweating) in m^2, λ the heat of vaporization of water at the measured surface temperature in $J \cdot kg^{-1}$ and dm/dt the evaporation rate of moisture leaving the thermal foot manikin's sweating surface in $kg \cdot s^{-1}$ [42].

In both cases, it is necessary to perform a test without the fabric, i.e., with just the black sock to determine the thermal insulation and with the black sock and the skin to determine the evaporative resistance. This method allows to determine the values of thermal insulation and evaporative resistance of the air layer. Subsequently, these values are subtracted from those obtained in the tests with the fabrics (i.e., total values), to have the fabric's thermal insulation and evaporative resistance values.

3.2.5 Preparation and application of IR reflectors formulations

The procedure for the preparation of the IR reflectors formulations used in the outer shell optimisation was developed by CeNTI and it is as follows:

1. Place the binding agent into a pre-weighed beaker and disperse with the wetting agent;
2. Add the first dose of the anti-foaming agent and disperse it until homogeneous;
3. Add the corresponding IR reflective pigment. The pigment mass calculation is in Appendix C;
4. Add the second dose of the anti-foaming agent;
5. Disperse until a vortex effect is clearly visible and until no more pigment particles remain to be dispersed. The evaluation of the dispersion is shown in Appendix D;
6. While the formulation is dispersing, add X g of thickening agent and 100 g of water in another beaker and mix slowly;
7. Add the previously prepared thickening agent and mix slowly;

After preparation, the formulation with the IR reflectors was applied to the outer shell using Mayer rods of 25 µm and 100 µm (Figure 6) to study the influence of the layer thickness of the formulation on its performance. The Mayer rods used are stainless steel rods tightly wound with stainless steel wire. This coating process consists of placing an excess of formulation on the substrate The formulation is spread by dragging the Mayer rod, and only the desired amount remains on the substrate. The amount of formulation remaining on the substrate is determined by the diameter of the wire that is around the rod [43].

Figure 6 – Mayer rods of 25 µm and 100 µm.

The curing of the fabrics with the IR reflectors formulations was done in an IV oven at a temperature of 85 ºC.

3.2.6 UV-Vis-NIR spectroscopy

In the characterisation of the outer shell with and without IR reflectors, the reflectance and colour differences of the surface were determined using a spectrophotometer Cary Series 5000. The spectrophotometer is equipped with a Labsphere RSA-PE-20 coupled 150 nm integrating sphere that allows measuring the ratio between the radiation reflected by the sample and the radiation reflected by a fully reflecting and perfectly diffusing standard under

equal irradiation and detection conditions. This is accomplished through a detector that quantifies the radiation reflected by the sample and the standard, as shown in Figure 7. Calibrating the equipment with the reference standard is crucial, since the measured reflectance is relative to the reference material [44].

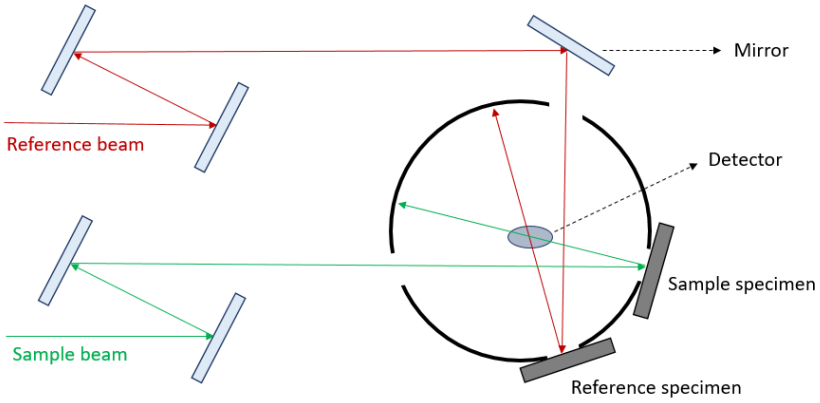

Figure 7 - *Diagram of the integrating sphere (adapted)* [44].

The reflectance was determined based on ASTM E 903 and the spectrum region considered for the study of the reflectance of the outer shell functionalized with IR reflectors was from 721 to 2500 nm, since it corresponds to the IR region [44].

The colour differences on the surface of the outer shell were determined using areflectance spectra in the visible range (i.e., between 400 and 720 nm), according to ASTM D 2244, interpreting in accordance with CIEDE2000 system (Appendix E) [45]. This system is based on three colour coordinates (L^*, a^* and b^*) and specifies the colour differences in a more sophisticated and computationally based way than the CIELAB system [46].

3.2.7 Construction of PCM pouches

Within the scope of this dissertation, two different ways of constructing PCM pouches were studied: manually and by bonding. In the manual construction of the PCMs pouches, the polymer X strips were cut with scissors and joined with polymer X adhesive. In the bonding construction method, an ExpressLaser GH1611TEL laser cutting machine was used to cut the polymer X strips. The laser used was a CO_2 laser and the optimised cutting speed was 10 mm/s. After cutting, the strips were bonded together in pairs using a Macpi pressing machine at a temperature of 160 ºC and a pressure of 6 bar. A 100 % polyurethane bi-adhesive film was used to bond the strips, which was pre-fixed to one of the strips for 15 seconds, and then bonded to the other strip for 30 seconds. The equipment used in this type of PCM pouch construction is shown in Figure 8.

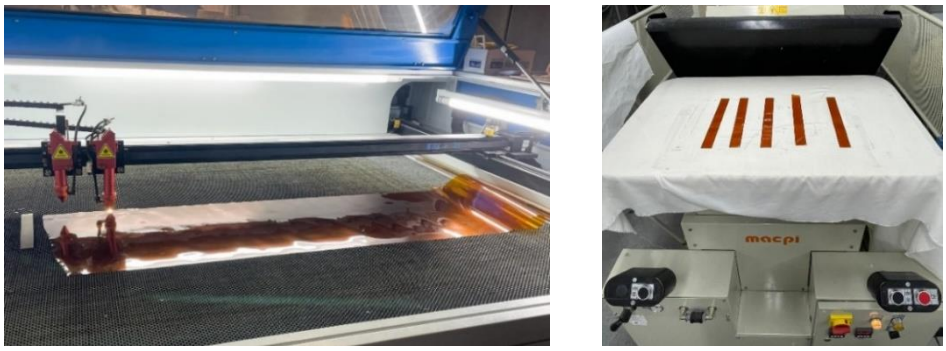

(a) (b)

Figure 8 - Bonding construction method: (a) laser cutting machine and (b) pressing machine.

Square 7 cm x 7 cm pouches and rectangular 7 cm x 3.5 cm pouches were constructed in order to evaluate the effect of the pouch geometry. In both methods, PCMs A and B were melted before being incorporated into the pouches, to have a more homogeneous PCMs distribution across the pouch. It was not necessary to melt PCM C since it was already a uniform powder.

3.2.8 Tensile tests

As the PCM pouches will be subjected to high-temperature variations when incorporated into the firefighter jacket, it is important to verify if their mechanical properties along their surface and junction zones will be compromised. Hence, tensile tests were carried out for determining the mechanical properties of polymer X strips and pouches on a Shimadzu AGX-50kNV testing machine (Figure 9), based on ASTM D882-10. These test consisted of applying a constant speed test of 71 $mm \cdot min^{-1}$ on polymer X strips and pouches with dimensions 2.5 cm x 24 cm until rupture. The speed test (i.e., rate of separation of the two grips) was based on a standard rule, which states that the speed test should be performed at half of the distance between grips (i.e., 142 mm).

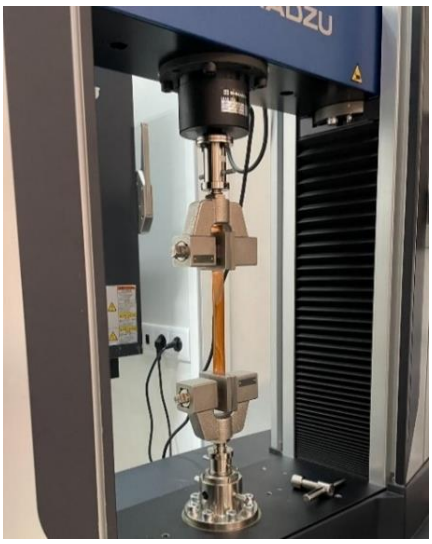

Figure 9 – Tensile test.

To evaluate the effect of temperature on the mechanical properties of polymer X, tests were carried out on strips and pouches with the same dimensions as in the previous tests at room temperature, at 50 ºC and at 80 ºC. Subsequently, the construction method effect on the mechanical properties of polymer X was also evaluated. Thus, tests were carried out at room temperature in pouches constructed manually and by bonding without and with 5 heat cycles of 5 minutes in the oven at 180 ºC.

3.2.9 Evaluation of transient behaviour

The evaluation of transient behaviour of the solution under study is imperative, since the implementation of PCMs implies a greater amount of accumulated heat in the garment which, as seen in section 2.3.3, can lead to third-degree burns in a post-exposure phase. For that reason, it is important to evaluate the behaviour of the solution under study during exposure and in a post-exposure phase. For this purpose, an experimental procedure was developed to evaluate the transient behaviour consisting of two different phases:

1. **Heating phase** - the sample is placed on between the installation table and the IR lamp, and therefore exposed to a constant radiant heat flux
2. **Cooling phase** - the sample is removed from the installation (i.e. not subjected to a heat flux) and is left to cool down to room temperature.

The installation used for the evaluation of the sample transient behaviour consists of a table and a Toshiba IR lamp at a height of 30 cm from the table top (Figure 10). The determination of the heat flux of IR lamps is in Appendix F. Additionally, a thermal camera is used to monitor the surface temperature of the sample using the infrared thermography technique (Appendix G) and data loggers to monitor the temperature on the inside face of the sample (Figure 11). The samples were placed in the laboratory 24 hours before testing, to ensure they were in equilibrium with ambient conditions at the start of the test.

Figure 10 - Installation for the evaluation of samples transient behaviour.

The final trials were performed with the PCMs pouches and the assembly (outer layer + PCM pouch + inner layer) insulated with XPS painted in white to prevent it from melting. The mass to surface area ratio of the PCM pouches was also considered, since the mass influences the amount of energy that the PCM will accumulate. Thus, a mass to surface area ratio of 0.38 $g \cdot cm^{-2}$ was used to make a comparative analysis of the efficiency of the PCMs. The experimental set-up for the transient behaviour evaluation tests is shown in Figure 11.

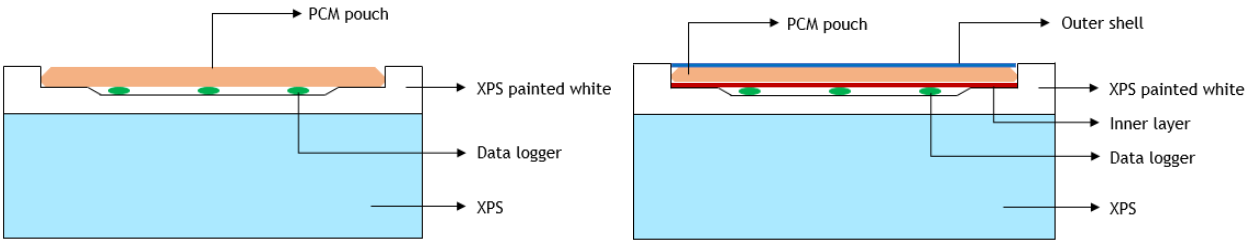

(a) (b)

Figure 11 - Schematic representation of the experimental set-up for the transient behaviour evaluation tests considering: (a) only the PCM pouch and (b) the assembly outer layer + PCM pouch + inner layer.

In the square PCM pouches, three data loggers were placed: a central one and two lateral ones. In the rectangular PCM pouches, only two data loggers were placed due to the space available on the pouch surface. The positioning of the data loggers in the square and rectangle pouches is shown in Figure 12 (a) and (b), respectively.

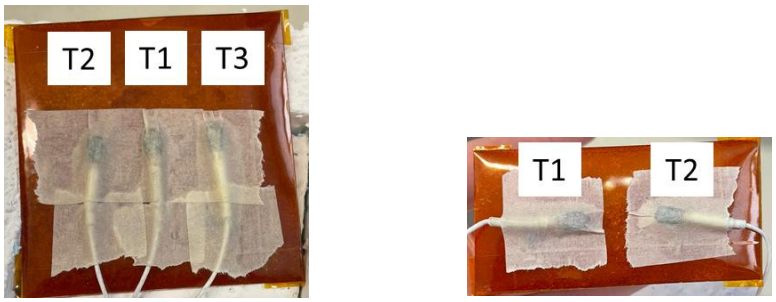

(a) (b)

Figure 12 - Positioning of the data loggers in the: (a) square pouch; (b) rectangle pouch.

This test was used to evaluate the transient behaviour of PCMs pouches with different geometries (square and rectangle), different types of PCMs and embedded in different assemblies of fabrics (i.e., outer shell with and without IR reflectors).

4 Results and discussion

The multilayer system under study consists of an outer shell (which may or may not be functionalised with IR reflectors), a pouch of PCMs and an inner layer. Thus, it was possible to study the effect of the application of IR reflectors in the outer shell and also the effect that the incorporation of PCMs can have on the thermal performance of the multilayer system for a firefighter's jacket. For this purpose, tests were conducted for both the fabrics and the PCM pouches individually and for the assembly. Throughout this chapter, the results concerning the tests performed will be presented and the possible integration of this multilayer system in a firefighter protective jacket will be discussed.

4.1 Fabrics

For the initial characterisation of the fabrics under study, the emissivity (ε), thickness (L), and weight were determined and are shown in Table 5.

Table 5 – Emissivity, thickness and weight of the fabrics and the respective standard deviations

Fabric	ε	L / mm	Weight / g·m^{-2}
Outer shell A	0.76 ± 0.01	0.39 ± 0.02	202.1 ± 0.2
Outer shell B	0.76 ± 0.02	0.41 ± 0.01	240.9 ± 0.3
Inner layer A	0.66 ± 0.02	0.90 ± 0.03	222.6 ± 0.2
Inner layer B	0.59 ± 0.01	1.22 ± 0.03	207.1 ± 0.2
Inner layer C	0.79 ± 0.01	0.29 ± 0.01	128.4 ± 0.1
Inner layer D	0.79 ± 0.02	0.27 ± 0.02	116.9 ± 0.1

From the analysis of Table 5, outer shells A and B are identical in emissivity and thickness, but outer shell B is heavier than outer shell A. Regarding the inner layers, as expected, the inner layers A and B are thicker and heavier than inner layers C and D, since they have an additional layer. It can also be observed that the emissivities of inner layers C and D are 0.13 and 0.20 higher than that of inner layers A and B, respectively, which means inner layers C and D absorb/emit significantly more energy as thermal radiation than inner layers A and B.

Subsequently, tests were performed with a thermal manikin in a controlled environment to determine the thermal insulation (I_t) and the evaporative resistance (R_e) of the fabrics under study. The moisture permeability index (I_{mp}) of the fabrics was determined through these two properties, using equation 1 of section 2.1.2. The results of thermal insulation, evaporative resistance and moisture permeability index of the fabrics under study are presented in Table 6.

Table 6 – Thermal insulation (I_t), evaporative resistance (R_e) and moisture permeability index (I_{mp}) of the fabrics and the respective standard deviations

Fabric	I_t / m²·ºC·W⁻¹	R_e / m²·Pa·W⁻¹	I_{mp}
Outer shell A	0.023 ± 0.002	6.568 ± 1.047	0.2078 ± 0.0385
Outer shell B	0.018 ± 0.001	5.816 ± 0.853	0.1825 ± 0.0278
Inner layer A	0.044 ± 0.001	1.224 ± 0.218	2.1564 ± 0.3854
Inner layer B	0.053 ± 0.003	4.806 ± 1.597	0.6689 ± 0.2251
Inner layer C	0.021 ± 0.002	1.080 ± 0.290	1.1518 ± 0.3315
Inner layer D	0.020 ± 0.001	1.361 ± 0.170	0.8916 ± 0.1278

Through the results in Table 6, outer shell A was chosen to integrate the multilayer system. This outer shell was chosen because, despite having a higher evaporative resistance than outer shell B, it has higher thermal insulation and moisture permeability index, which provides a faster rate at which sweat will evaporate and transported through the fabric. In addition, as seen earlier, outer shell A is also lighter than outer shell B. Regarding the inner layers, according to the requirements described in ISO 15384, the maximum thermal insulation of a firefighter's protective clothing for wildland fires is 0.055 $m^2 \cdot ºC \cdot W^{-1}$. Thus, it can be concluded from the results of Table 6 that the inner layers A and B cannot be used in the multilayer system under study, since when combined with an outer shell, they would exceed the maximum value of thermal insulation required by the standard. Yet, they might be a valid option for a multilayer system intended for structural fires, since EN 469 has no maximum thermal insulation limit. As the inner layers C and D have very similar thermal insulations, C was chosen as the inner layer for the multilayer system as it has a lower evaporative resistance and a higher permeability index.

4.2 IR reflectors

The functionalisation of the outer shell under study was done by applying IR reflector formulation with a thickness of 25 µm and 100 µm. The outer shells without and with IR reflectors are shown in Figure 13.

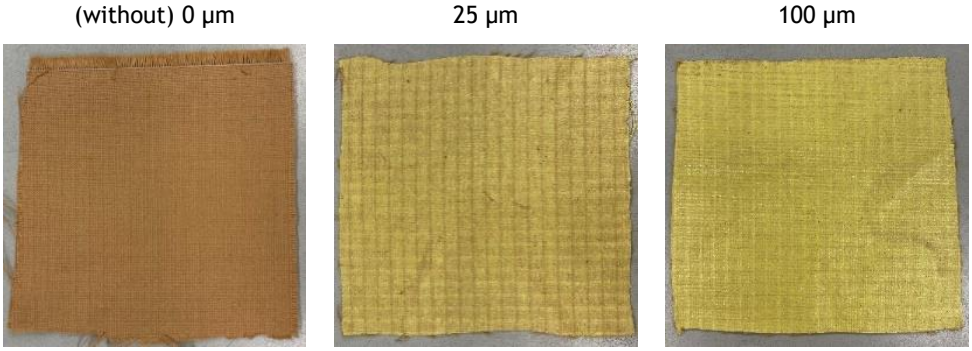

Figure 13 - Outer shells without and with 25 µm and 100 µm IR reflector formulation.

From Figure 13, it can be seen that in the outer shell with 25 um of IR reflector formulation the substrate rows were not coated (i.e., uncovered lines of the substrate are visible). However, it is observed that the colour of both outer shells changed significantly, which may be a drawback since there are restrictions on the colours of firefighter's jackets.

Subsequently, the lightness difference ($\Delta L'$), the chroma difference ($\Delta C'$) and the colour difference (ΔE_{2000}) of the functionalised outer shells surfaces were determined and are listed in Table 7.

Table 7 – Lightness difference ($\Delta L'$), chroma difference ($\Delta C'$) and colour difference (ΔE_{2000}) of the functionalised outer shells surfaces

Outer shell	$\Delta L'$	$\Delta C'$	ΔE_{2000}
A	-	-	-
A + 25 µm	14,8	12,0	14,7
A + 100 µm	19,3	17,4	18,0

Through the analysis of Table 7, it can be concluded that the greater the applied thickness of the formulation with IR reflectors, the brighter and more saturated the surface of the functionalized outer shell is. This means that the greater the amount of IR reflectors, the greater the colour difference in relation to the non-functionalised outer shell.

Following this, the reflectance of the outer shells under study was also determined. Figure 14 shows a comparison between the mean value of the reflectance of the outer shells without and with IR reflectors (2 tests) and the respective standard deviation.

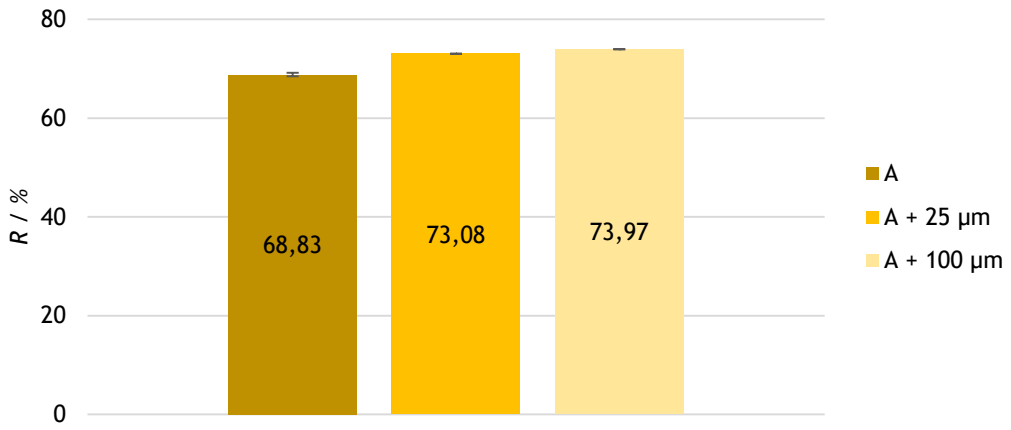

Figure 14 - Reflectance of outer shells without and with IR reflector formulation (25 µm and 100 µm).

Through the analysis of Figure 14, it can be concluded that the reflectance of the outer shell A increased by 6.2 % and 7.5 % with the application of 25 µm and 100 µm of IR reflector formulation, respectively. However, it can be seen that the variation in reflectance between 25 µm and 100 µm is not significant, with the difference being only 1.3 %.

A test was performed on the installation of the IR lamps with the same configuration as in the tests for evaluation of the transient behaviour (i.e., one lamp at the height of 30 cm from the table top) to verify the potential of the functionalised outer shells in delaying the heating of the substrate. This test consisted of heating the outer shells for three minutes, controlling the surface temperature through the thermal camera. The temperature profiles obtained in the outer shells surfaces with and without IR reflectors and the respective standard deviations are shown in Figure 15.

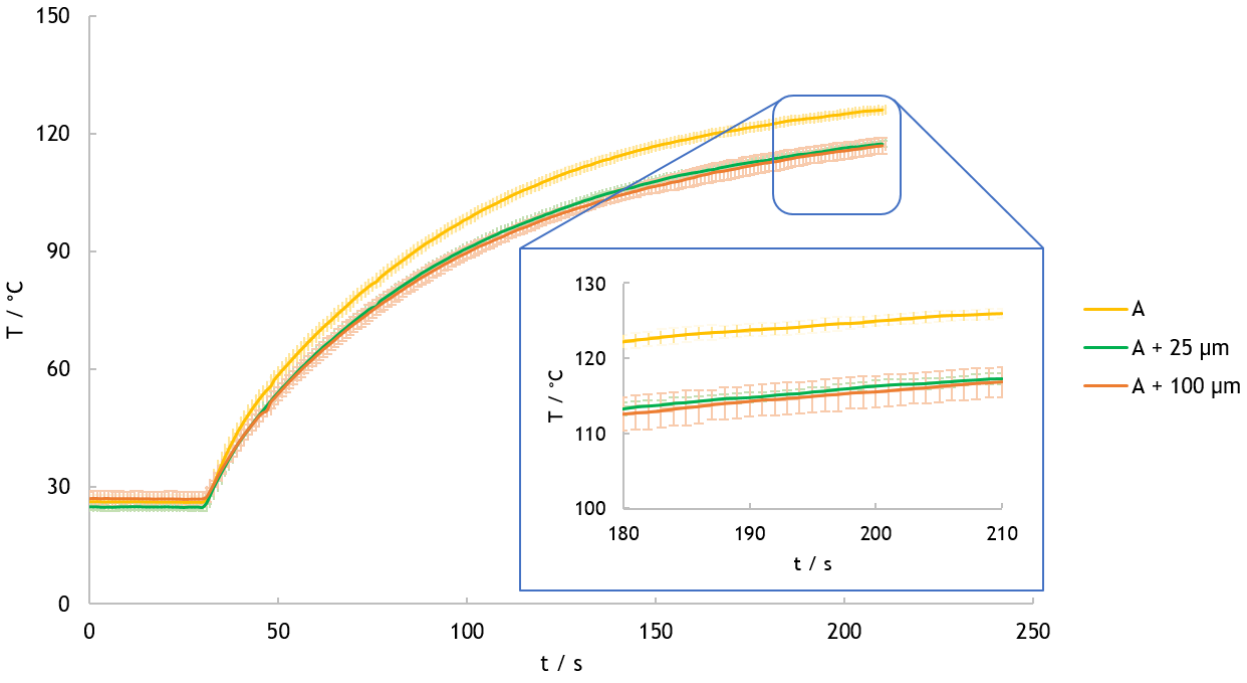

Figure 15 - Effect of IR reflectors formulation on the temperature profiles obtained in the outer shells surfaces.

In Figure 15, it can be seen that the application of 25 µm and 100 µm of IR reflector formulation implies a decrease of 8.7 ºC and 9.1 ºC, respectively, in the surface temperature of the outer shell after three minutes of exposure. However, it can be noted that the difference between 25 µm and 100 µm is not significant, implying a difference in the heating delay of the outer shell surface of only 0.4 ºC.

The evaporative resistance of each of the fabrics, with and without IR reflectors, was determined to understand the impact of the application of the formulation with IR reflectors on the thermophysiological comfort of the firefighter protective clothing. Figure 16 shows the evaporative resistance of the outer shells under study and the respective standard deviations.

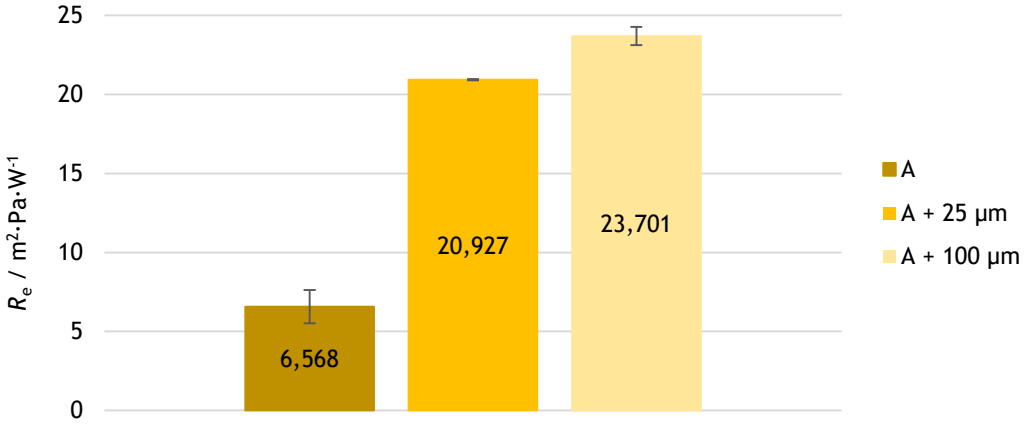

Figure 16 – Evaporative resistance of outer shells without and with 25 µm and 100 µm IR reflector formulation.

From Figure 16, it can be seen that the evaporative resistance of outer shell A without IR reflectors is 6.569 m^2·Pa·W^{-1} and when 25 µm and 100 µm of IR reflectors formulation were applied it increased to 20.927 m^2·Pa·W^{-1} and 23.701 m^2·Pa·W^{-1}, respectively. However, according to ISO 15384, the evaporative resistance of a firefighter's protective clothing for wildland fires must be less than or equal to 10 m^2·Pa·W^{-1}. That being said, it can be seen from Figure 16 that the use of formulations with IR reflectors is not viable for the desired solution, as the evaporative resistance of the outer shells with IR reflectors is more than twice the value of the maximum limit required by the standard. However, it may be a viable option for a structural and proximity firefighter's protective jacket, as according to EN 469 the maximum evaporative resistance is 30 m^2·Pa·W^{-1} for this equipment.

4.3 Polymer X's mechanical properties

The mechanical properties of polymer X strips and pouches were determined by means of tensile tests, which response is a stress-strain curve. Through these tests, Young's modulus (i.e., the slope of the line zone of the elastic region), tensile strength (i.e., stress at rupture point) and ductility (i.e., strain at rupture point) were determined. Figure 17 is an example of a stress-strain curve from a test performed on polymer X and the demonstration of how these mechanical properties are determined.

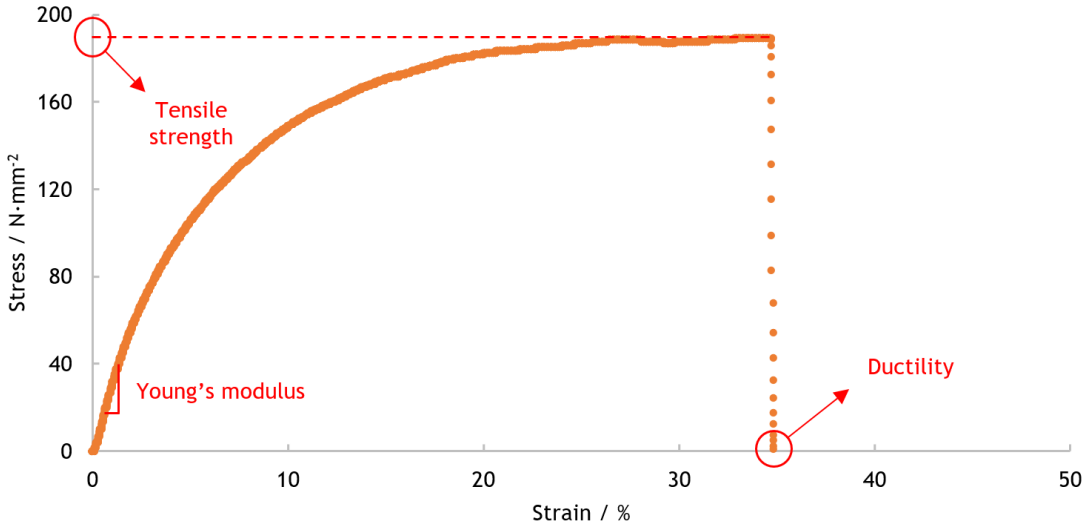

Figure 17 - Example of a stress-strain curve from a test performed on polymer X.

The results shown in the following subchapters were determined using stress-strain curves. However, for the sake of conciseness, the curves are presented in Appendix H.

4.3.1 Influence of temperature

As the PCMs pouches will be subject to high-temperature variations, it was important to verify the effect of these variations on the mechanical properties of the pouch material, i.e., the polymer X. Thus, Young's modulus, tensile strength and ductility of the strips and pouches were determined at different temperatures. The Young's modulus of the strips and pouches and the standard deviation are shown in Figures 18 (a) and (b), respectively, at room temperature, 50 ºC and 80 ºC.

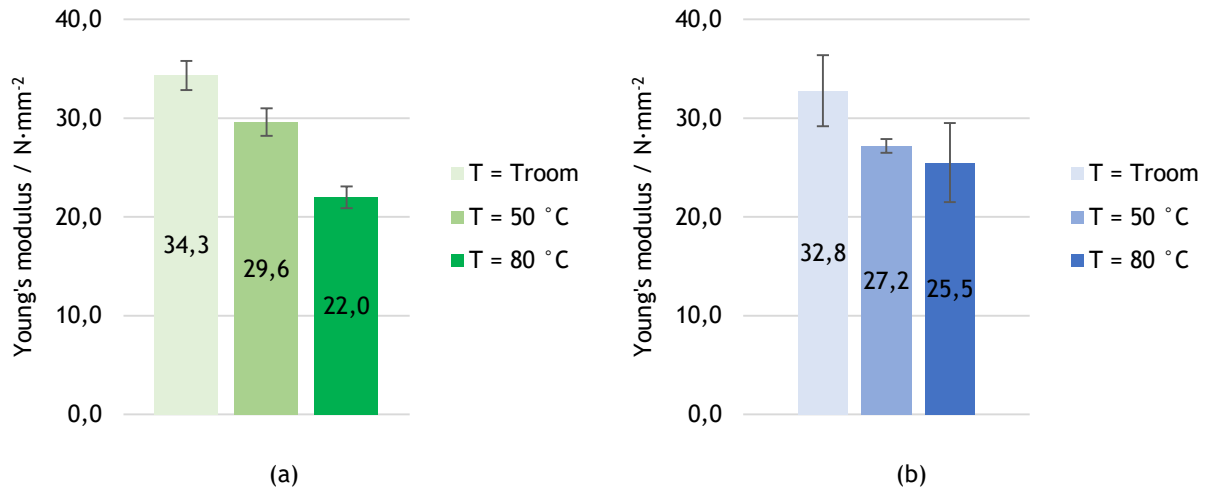

Figure 18 - Influence of temperature on Young's modulus of: (a) strips and (b) pouches.

For the strips of Figure 18 (a), it can be seen that a temperature increase from room temperature to 80 ºC implies a decrease of 12.3 $N \cdot mm^{-2}$ in Young's modulus of the material. By comparison, the pouches of Figure 18 (b) show a smaller decrease in Young's modulus of only 7.3 $N \cdot mm^{-2}$. This behaviour was expected as increasing temperature causes an increase in atomic thermal vibrations, leading to weaker secondary bonds and hence a softer polymer [47].

Figure 19 (a) and (b) shows the tensile strength of the strips and pouches and its standard deviation, respectively, at room temperature, 50 ºC and 80 ºC.

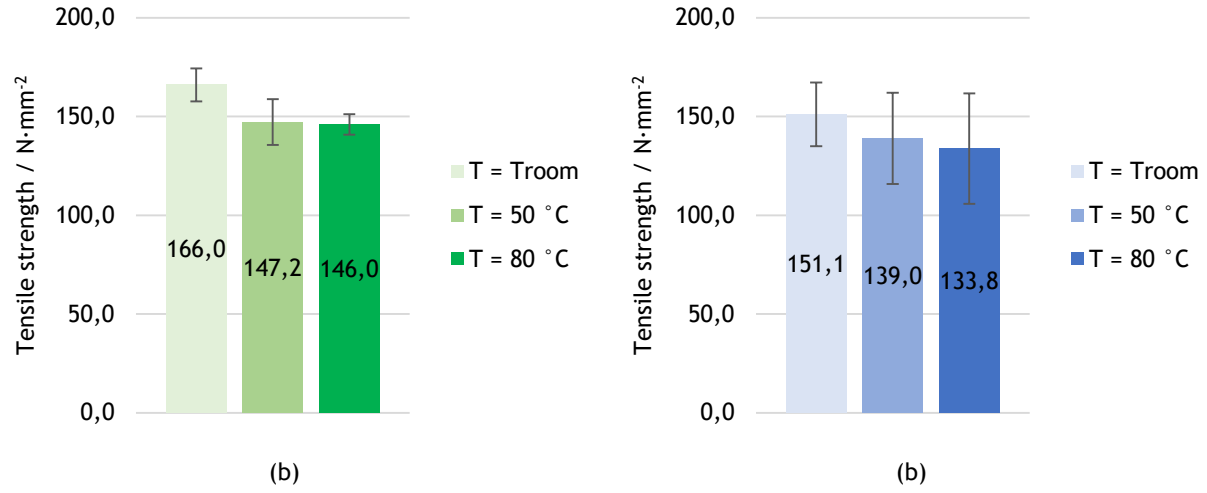

Figure 19 - Influence of temperature on tensile strength of: (a) strips and (b) pouches.

From Figure 19, it can be concluded that there is a decrease of 20.0 $N \cdot mm^{-2}$ and 17.3 $N \cdot mm^{-2}$ in the tensile strength of the strips and pouches, respectively, when subjected to a temperature increase from room temperature to 80 ºC. This behaviour was expected, since an increase in temperature increases the mobility of the molecular chains, decreasing the strength of the polymer [48]. Furthermore, the tensile strength of the pouches is 14.9, 8.2 and 12.2 $N \cdot mm^{-2}$ lower than that of the strips at room temperature, 50 ºC and 80 ºC, respectively, which might have to do with the presence of the adhesive at the junctions of the pouches.

The ductility of the strips and pouches and the standard deviation are shown in Figure 20 (a) and (b), respectively, at room temperature, 50 ºC and 80 ºC.

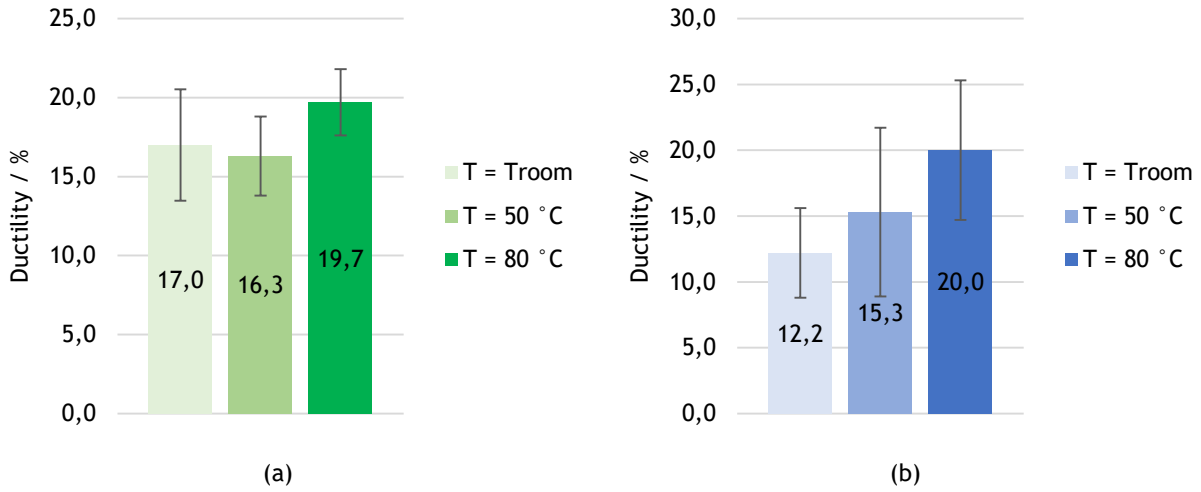

Figure 20 - Influence of temperature on the ductility of: (a) strips and (b) pouches.

From Figure 20 (a), it can be noted that a temperature increase from room temperature to 80 ºC implies an increase of 2.7 % in the ductility of the material. By comparison, the pouches of Figure 18 (b) show a greater increase in ductility of 7.8 %. Ductility is expected to increase with temperature increase, since by increasing the mobility of the molecular chains, the polymer is able to elongate more [48].

4.3.2 Comparison of construction methods

In addition to the influence of temperature, it was also assessed whether the construction method (i.e., manual or by bonding) influences Young's modulus, tensile strength and ductility of the pouches. Furthermore, the pouches were previously exposed to heat cycles to evaluate their effect on the material's mechanical properties. Therefore, Young's modulus, tensile strength and ductility were determined at room temperature for pouches constructed manually and by bonding with and without heat cycles. Figure 21 shows the comparison of Young's modulus and the standard deviation between pouches with and without heat cycles constructed manually and by bonding.

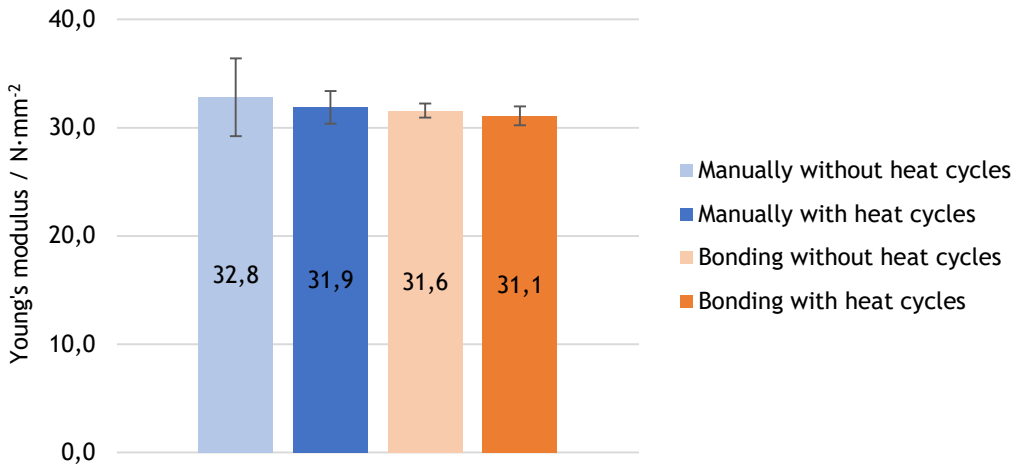

Figure 21 - Young's modulus of the pouches constructed by different methods, with and without heat cycles.

By the analysis of Figure 21, it is concluded that Young's modulus does not vary significantly neither with the construction method nor with the heat cycles (maximum deviation of 0.9 $N \cdot mm^{-2}$). It is also observed that the Young's modulus values of manually constructed pouches are similar to those of pouches constructed by bonding.

The comparison of tensile strengths and the respective standard deviations between pouches without and with heat cycles constructed manually and by bonding is shown in Figure 22.

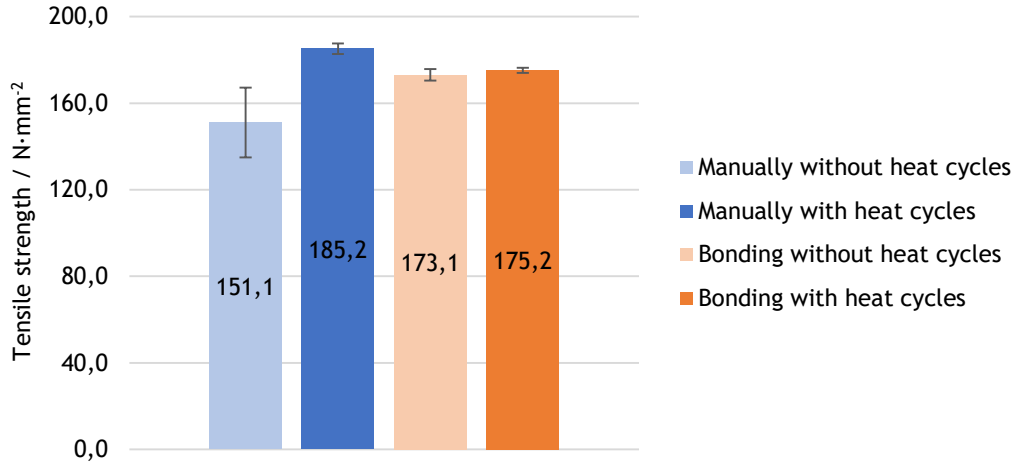

Figure 22 – Tensile strength of the pouches constructed by different methods, with and without heat cycles.

In Figure 22, a significant increase of 34.2 $N \cdot mm^{-2}$ is observed in the tensile strength of the hand-built pouches after heat cycles. One possible explanation for this behaviour is the detachment of the adhesive, which was visible in some tests on the pouches with heat cycles. As seen in section 4.2.1, it is likely that the adhesive confers some fragility to the pouches. Therefore, the detachment of this might eliminate this fragility, leading to a higher tensile strength. Also, it can be noted that the heat cycles did not significantly influence the tensile strength of the pouches constructed by bonding (deviation of only 2.1 $N \cdot mm^{-2}$).

In Figure 23 is presented the comparison of ductility and its standard deviation between pouches without and with heat cycles constructed manually and by bonding.

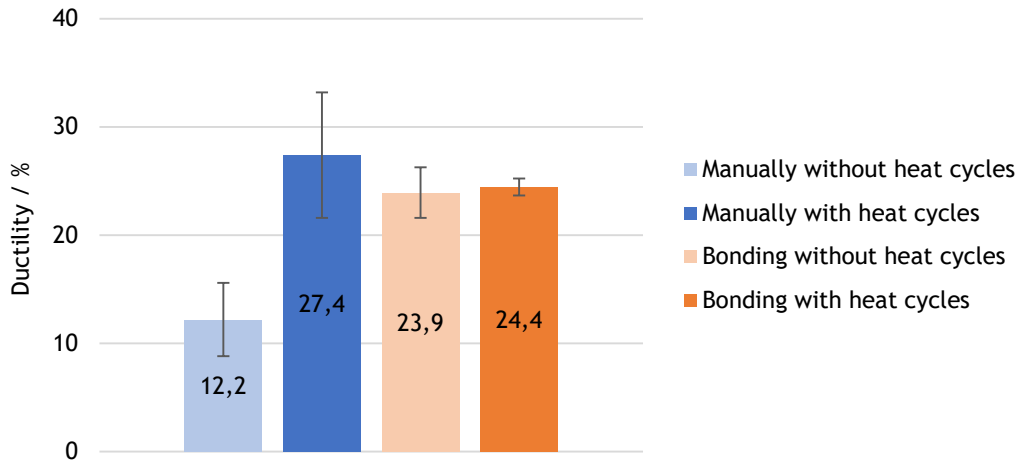

Figure 23 - Ductility of the pouches constructed by different methods, with and without heat cycles.

In Figure 23, it can be noted that the exposure to heat cycles caused a 15.2 % increase in ductility in the manually constructed pouches. However, the ductility of the pouches constructed by bonding did not vary significantly with heat cycles, with a deviation of only 0.5 %.

Both construction methods proved to be adequate for the final application. Manual construction presents itself as a simpler method and with less equipment needed. However, the results showed lower reproducibility (i.e., higher standard deviations). As an alternative, bonding is a construction method with more specific and less available equipment, but that ensures higher reproducibility. Since this analysis was made at different times due to the availability of equipment, manual construction pouches were used in the subsequent studies despite their lower reproducibility.

4.4 PCM pouches thermal performance

The test described in section 3.2.9 was performed on square and rectangular pouches to study the transient behaviour of PCM pouches. The ambient test conditions for the transient behaviour evaluation of PCM pouches can be found in Appendix I.

4.4.1 PCM A

PCM A is the PCM with the melting point closest to the pain threshold temperature and the one with the highest latent heat of fusion (Table 3). Therefore, PCM A is the PCM with the capacity to store a more significant amount of energy during fusion.

The tests with PCM A were carried out at an ambient temperature between 24.1 and 25.5 ºC and a relative humidity between 54.8 and 61.0 %. The stopping criterion for the test with PCM A was 85 ºC in one of the data loggers, which corresponds to its maximum operating temperature. Figure 24 shows the temperature profile registered during the evaluation of the transient behaviour of PCM A for both geometries. The solid line is the mean value of the temperature of each data logger after two tests and the area around the solid line with the same colour is the respective standard deviation.

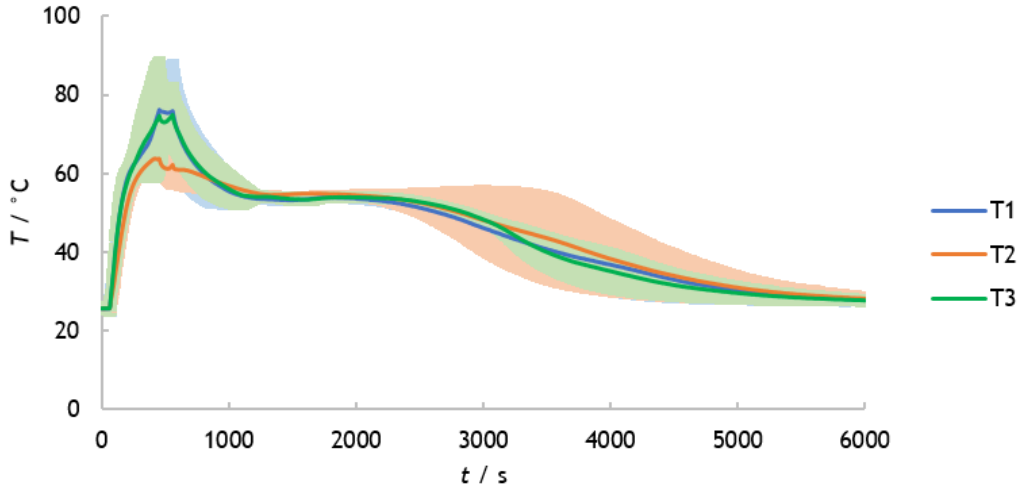

(a)

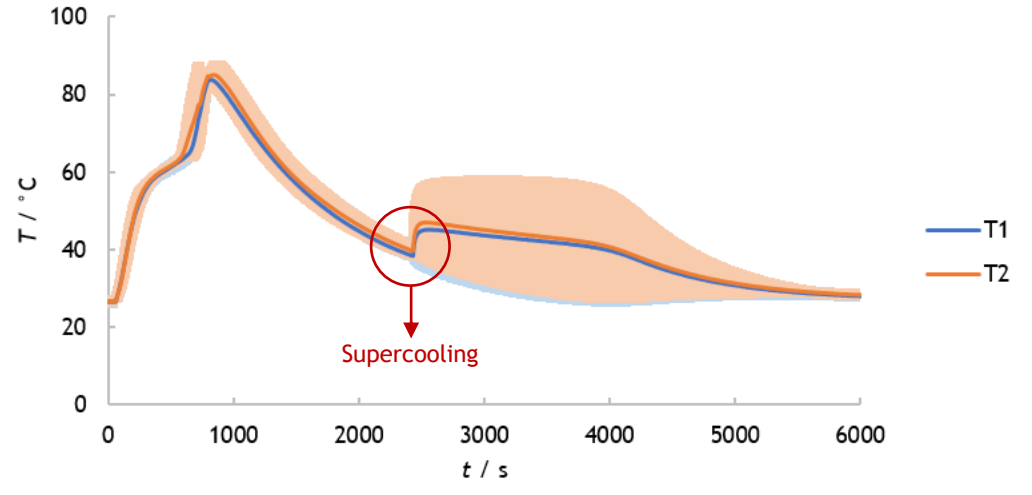

(b)

Figure 24 - Temperature profile of PCM A in (a) square pouch and (b) rectangle pouch registered during the evaluation of the transient behaviour.

Figure 24 (a) shows that the temperature of data logger T2 did not reach high temperatures like data loggers T1 and T3, due to the existence of an air bubble above these data loggers (visible in Figure 25). As a result, the PCM of the square pouch was not able to melt fully.

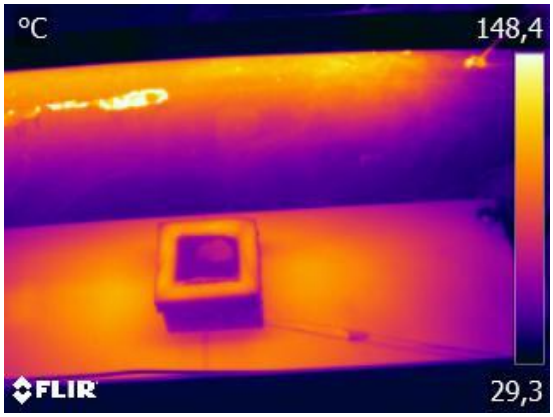

Figure 25 - Thermal camera image of the square pouch with PCM A at t = 4 min

Regarding the rectangular pouch, in the first test, the PCM melted completely and, due to the low rate of crystal formation, supercooling did occur (this possibility is considered in the product sheet). This phenomenon is marked in Figure 24 (b) and results in the melting temperature being higher than in the solidification temperature. In the second test, the PCM did not solidify and, consequently, did not present solidification step. This behaviour was also seen in preliminary tests with square pouches after supercooling occurred, which might indicate that there is degradation of PCM after supercooling.

4.4.2 PCM B

PCM B is of similar nature to PCM A, but it has a higher melting point and a lower latent heat of fusion (Table 3).

The tests with PCM B were carried out at an ambient temperature between 22.8 and 24.2 ºC and a relative humidity between 47.2 and 59.8 %. The stopping criterion for the test with PCM A was 90 ºC in one of the data loggers, which also corresponds to its maximum operating temperature. The profile temperature registered during the evaluation of the transient behaviour of PCM A for both geometries is shown in Figure 26. The solid line is the mean value of the temperature of each data logger after two tests and the area around the solid line with the same colour is the respective standard deviation.

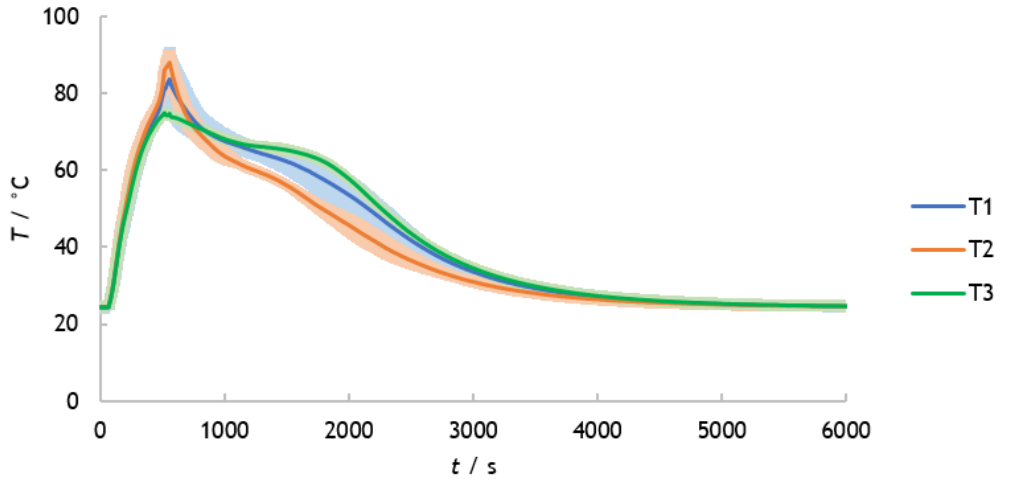

(a)

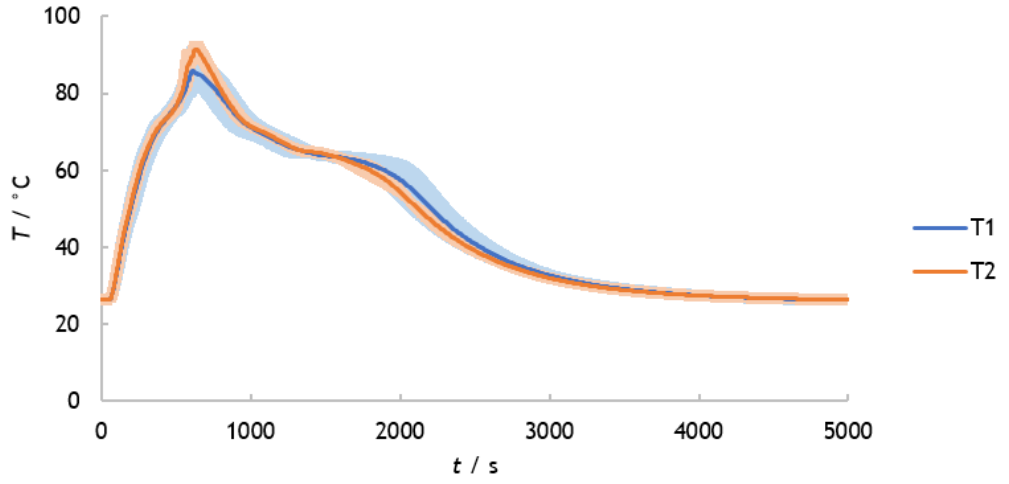

(b)

Figure 26 - Temperature profile of PCM B in (a) square pouch and (b) rectangle pouch registered during the evaluation of the transient behaviour.

Like PCM A, the square pouch of PCM B also contained an air bubble, which is visible in Figure 27 (a). It was visually observed in the first test that the air bubble was above the data loggers T1 and T2, but in the second test it moved only above the data logger T2. It is possible to see in Figure 26 (a) the influence of this air bubble on the temperature of data logger T2, which on average reaches temperatures of 90 ºC while data loggers T1 and T3 reach 84 ºC and 75 ºC, respectively. Consequently, the melting and solidification steps of the square pouch are not evident. However, in the rectangle pouch you can identify a melting step between 350 and 550 seconds and a solidification step between 1000 and 1800 seconds in Figure 26 (b). This behaviour happens because, besides the existing bubble (visible in Figure 27 (b)) not being above the data loggers, this pouch has a greater thickness of PCM (the thickness of the square pouch varies between 3.23 and 4.27 cm, while the thickness of the rectangular pouch varies between 6.07 and 6.17 cm).

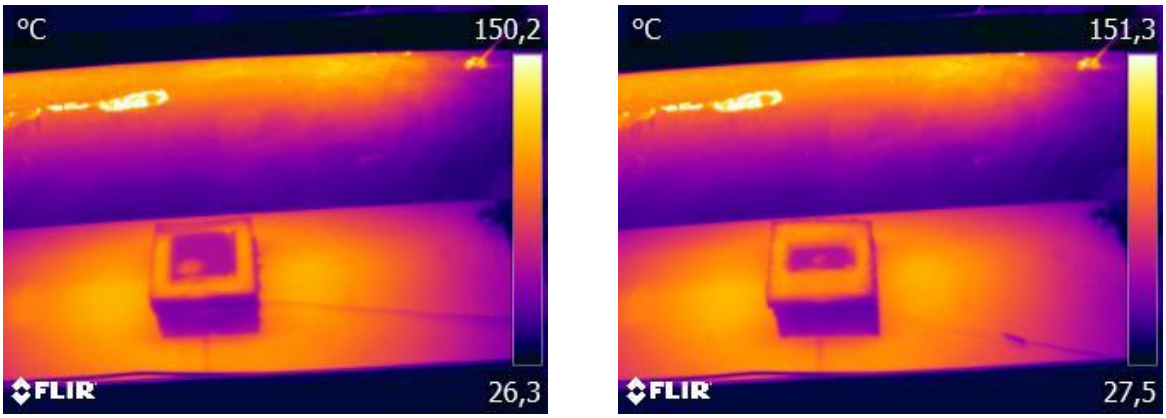

(a) (b)

Figure 27 - Thermal camera image of the: (a) square pouch and (b) rectangular pouch with PCM B at *t* = 4 min

4.4.3 PCM C

PCM C is a heat storage powder that contains phase change material (PCM) within a secondary supporting structure, in this case, a hydrophilic silica powder. This PCM has the great advantage of not having to be melted before being incorporated into the pouches, allowing for easier construction.

The tests with PCM C were carried out at an ambient temperature between 22.5 and 25.0 ºC and a relative humidity between 56.9 and 61.1 %. The stopping criterion for the test with PCM C was 95 ºC in one of the data loggers, since the white-painted XPS used as insulation (Figure 11) melted when the temperature of one of the data loggers reached the maximum operating temperature of this PCM, which is 110 ºC. Figure 28 shows the temperature profile registered during the evaluation of the transient behaviour of PCM C for both geometries. The solid line is the mean value of the temperature of each data logger after two tests and the area around the solid line with the same colour is the respective standard deviation.

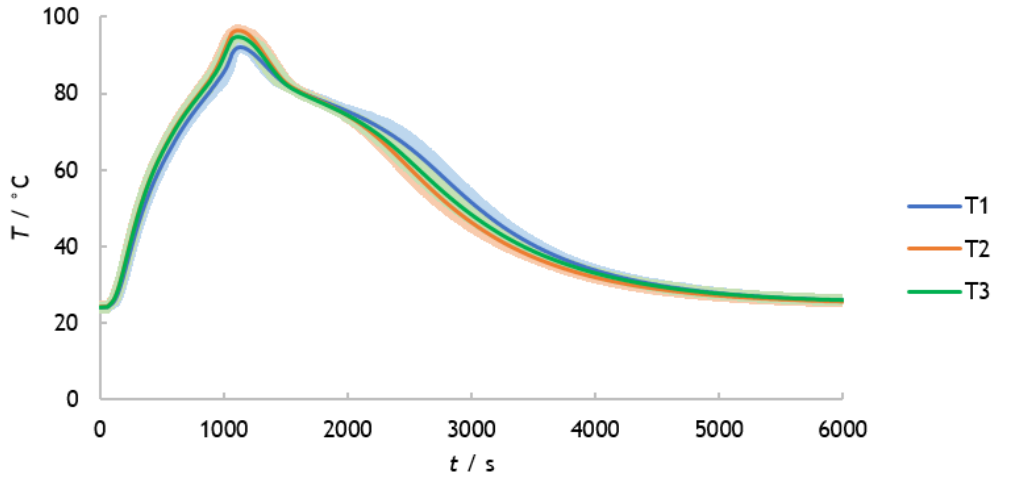

(a)

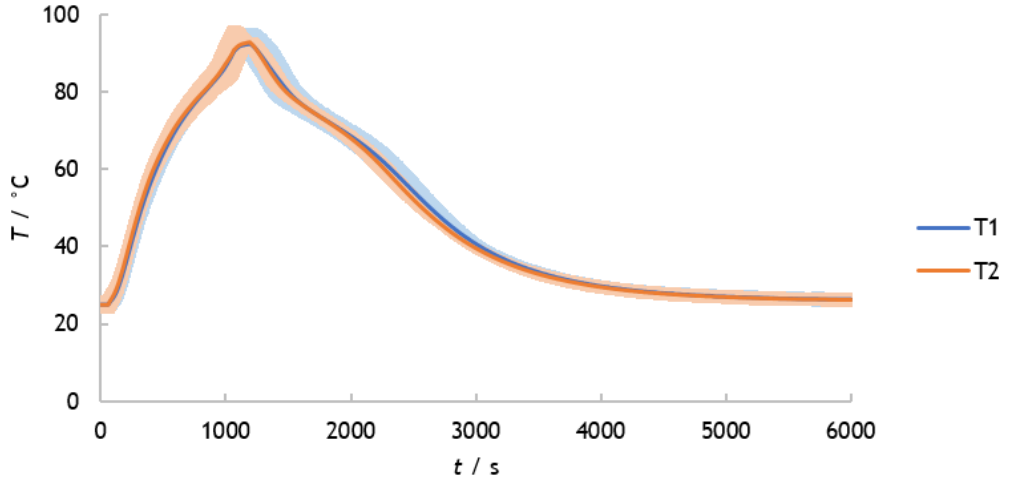

(b)

Figure 28 - Temperature profile of PCM C in (a) square pouch and (b) rectangle pouch registered during the evaluation of the transient behaviour.

From Figure 28, no significant differences are observed in the temperature profile between the geometries. Also, it can be seen that there is greater homogeneity in the way this PCM spreads across the pouch, since it is the only PCM that presents coincident temperature profiles in the various points analysed. This homogeneity becomes even more evident when observing the images obtained through the thermal camera (Figure 29), where a more homogeneous temperature is seen on the surface of the pouch. However, the melting and solidification step is hardly visible, which might be because these pouches contain only 60 % of PCM and the other 40 % correspond to silica powder. This means that, in essence, the ratio of PCM mass per surface area of the pouch is not the same as in the other PCM pouches. However, the pouches with PCM C were already practically full (i.e., with the maximum amount of PCM that can be introduced into the pouch), meaning that it would not be possible to have a real ratio between the mass of PCM and the surface area of the pouch of 0.38 for this PCM by the same construction method.

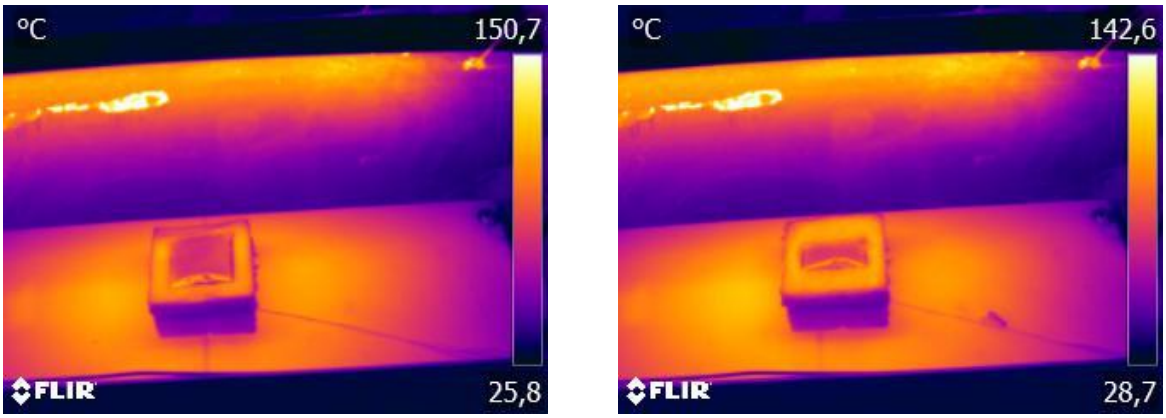

(a) (b)

Figure 29 - Thermal camera image of the: (a) square pouch and (b) rectangular pouch with PCM C at *t* = 4 min

4.4.4 Comparison between PCMs

The results obtained on the square PCM pouches were considered to study the influence of PCMs on pouches thermal performance, since they provide the most homogeneous distribution of temperature. This homogeneity can be verified through the figures in Appendix J, where higher heat transfer rates through the sideswalls can be seen in the rectangles. PCM A was not included in this analyses, since it did not fully melt (Figure 24 (a)) and so the temperature profiles obtained on the pouch surface are not comparable to the others. The comparison of the temperature profiles during the evaluation of the transient behaviour between PCM B and C is found in Figure 30. This figure contains the mean value (solid line) of the temperatures of the three data loggers of two tests and the respective standard deviations (area around the solid line with the same colour).

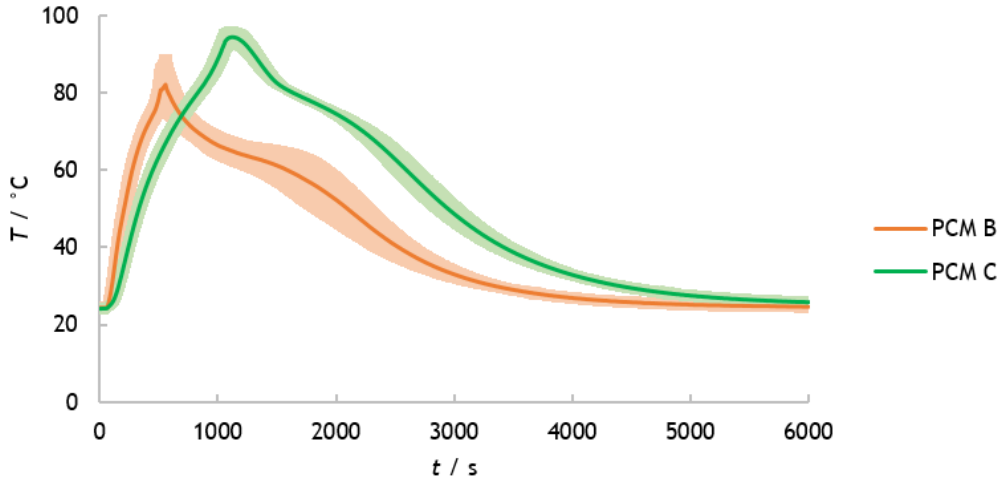

Figure 30 - Temperature profiles registered during the evaluation of the transient behaviour with different PCMs.

From Figure 30, it can be seen that PCM C, despite a lower ratio between the mass of PCM and the surface area of the pouch, it exhibits slower heating and cooling than PCM B. This behaviour can be explained by the fact that PCM C has a thermal conductivity six times lower than PCM B, since they have equal specific heats (Table 3). The density of PCMs can also influence their heating and cooling rates. However, the supplier did not provide this information and, therefore, the effect of density on the heating and cooling rates of the PCMs could not be analysed. Furthermore, PCM C is more homogeneous, as seen in section 4.3.3, and easier to incorporate into pouches as it is already a uniform powder. For these reasons, the PCM chosen for the multilayer system was PCM C.

4.5 Multilayer system

The outer shell chosen was A, to verify the application effect of an IR reflector formulation on the heating delay of the assembly. The outer shell functionalised with IR reflector chosen was the one with a thickness of 25 µm, since it was concluded that it has similar performance in terms of heating delay to the 100 µm thickness and it has the advantage of having a lower evaporative resistance (Figure 16). Regarding the intermediate layer, the PCM chosen was C, since it exhibits a more homogeneous spread across the pouch and it is easier to incorporate into the pouches than the other PCMs studied. PCM C was incorporated into manually constructed pouches due to time and resource constraints. Moreover, square pouches were used, as this geometry has a temperature distribution more homogeneous. Lastly, the inner layer chosen was C, due to the maximum thermal insulation limit required by ISO 15384 and because it has lower evaporative resistance and a higher moisture permeability index than inner layer D.

The effect of applying IR reflectors to the outer shell of the assembly on the temperature profile is presented in Figure 31. The solid line is the mean value of the temperatures of the three data loggers of two tests and the area around the solid line with the same colour is the respective standard deviation. The tests were performed at ambient temperatures between 23.5 and 25.4 ºC and relative humidity between 56.9 and 60.9 % (Appendix I).

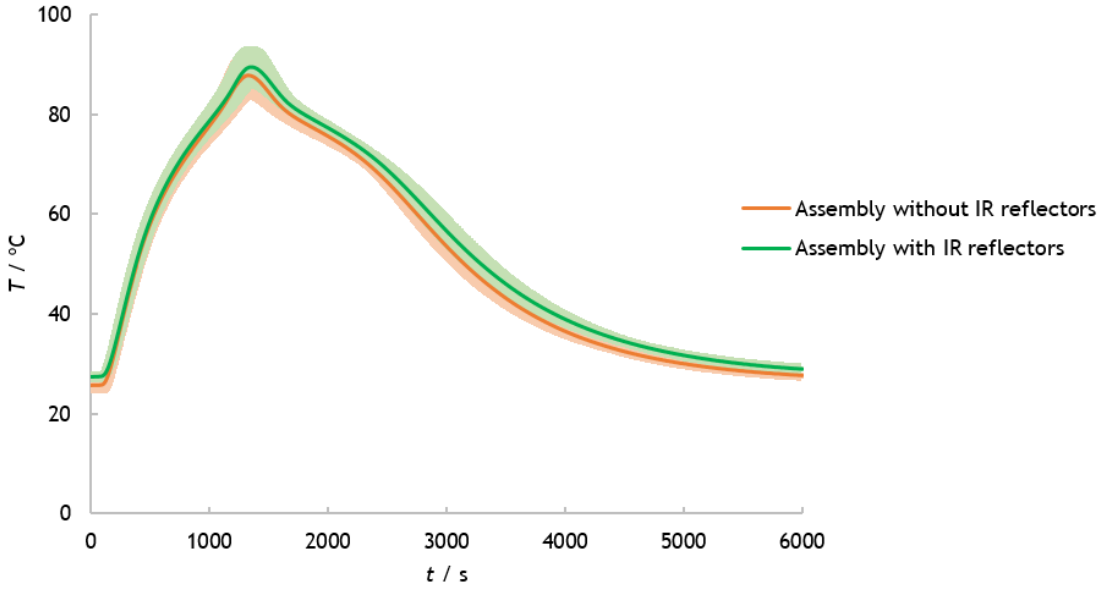

Figure 31 - Effect of the presence of IR reflectors on the temperature profiles of the multilayer system.

In Figure 31, it can be seen that the assemblies without and with IR reflectors have similar behaviour, with an initial heating rate of 0.09 ± 0.01 ºC·s^{-1} in both assemblies. Based on this, it is concluded that the best option for the multilayer system for the firefighter jacket is the assembly without IR reflectors, since it has similar thermal performance to the assembly with IR reflectors, but has a lower evaporative resistance (Figure 16). It was not possible to test the evaporative resistance of the assemblies during this dissertation. However, it is possible to state that the evaporative resistance of the assembly without IR reflectors is lower than that of the assembly with IR reflectors, since all layers are common to both assemblies, with the exception of the outer shell that has an additional layer with IR reflectors (tested in chapter 4.4).

The effect of the incorporation of PCM C on the temperature measured by the data loggers is presented in Figure 32. The tests were performed at an ambient temperature between 23.5 and 25.9 ºC and a relative humidity between 58.1 and 60.9 % (Appendix I).

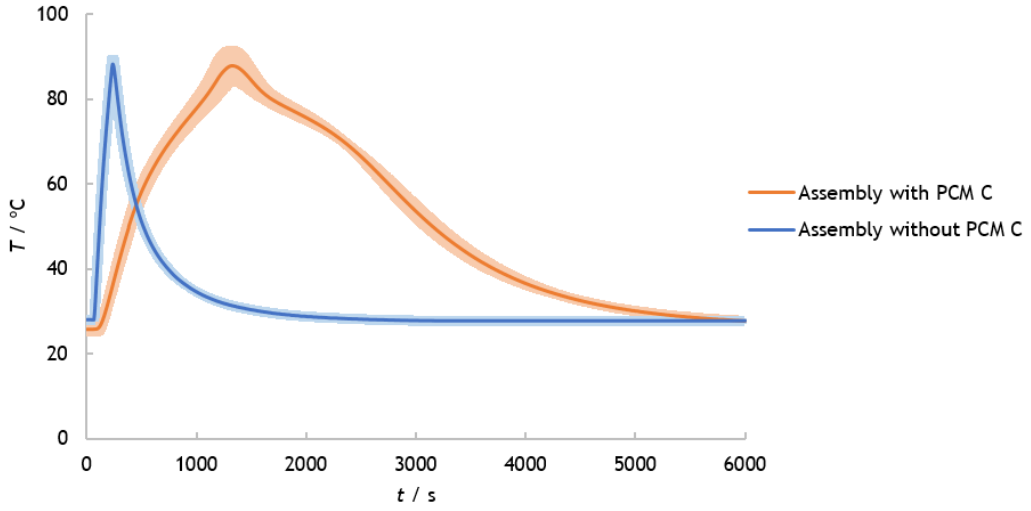

Figure 32 - Effect of the incorporation of PCM C on the temperature profiles of the multilayer system.

From Figure 32, it can be seen that the behaviour of the assembly without PCMs is different from the assembly with PCMs. During the exposure to the radiant heat flux, the assembly without PCM C (i.e., consists only in an outer shell and an inner layer) shows an increase in heating rate significantly sharper than the increase rate obtained for the assembly with PCM C, with an initial heating rate of 0.44 ± 0.01 $^{o}C \cdot s^{-1}$. As previously mentioned, the initial heating rate of the assembly with the incorporated PCMs is 0.09 ± 0.01 $^{o}C \cdot s^{-1}$, which corresponds to a decrease of 79.5 %. This decrease is due to the fact that the assembly with PCM C has an additional layer, which provides higher thermal insulation (due to the addition of both PCM and pouch material). Nevertheless, the effect of PCM latent heat on the pouch temperature is not significant. Further studies considering a large amount of PCM should be interesting to study. Although the incorporation of PCMs is beneficial since it decreases the heating rate of the assembly, it also dramatically delays its cooling by almost 4500 seconds. Furthermore, it is important to emphasise that the incorporation of PCMs in the firefighter jacket also increases its weight and evaporative resistance.

5 Conclusion

With the purpose of developing an innovative firefighter jacket for wildland fires, a multilayer system integrated PCMs was studied at small scale. Within the scope of this dissertation, an experimental procedure was also developed to evaluate the transient behaviour of PCMs pouches and the multilayer system, simulating the different phases that a firefighter is exposed to in firefighting.

The developed multilayer system consists of three layers: an outer shell, a PCM pouch and an inner layer. Among the outer shells studied, outer shell A was chosen to integrate the multilayer system, since it has a high thermal insulation and moisture permeability index, providing a faster rate at which sweat will be evaporated through the fabric. This outer shell was also functionalised with IR reflectors to increase its reflectance and, consequently, delay the assembly's heating. Thus, 25 µm and 100 µm of IR reflector formulation were applied to the outer shell and, after the tests presented in chapter 4.4, it was concluded that the thickness of 25 µm is the one that had the best risk-benefit ratio. Regarding the PCMs, PCM C showed the most promising results, since it presented a greater homogeneity in the way its spreads across the pouch and an easier method of incorporation into the pouches. Concerning the pouch construction, both methods proved to be adequate for the final application. Manual construction presents itself as a simpler method and with less equipment needed. However, the results showed lower reproducibility (i.e., higher standard deviations). As an alternative, bonding is a construction method with more specific and less available equipment, but that ensures higher reproducibility. Lastly, the inner layer chosen was C due to the maximum thermal insulation limit required by ISO 15384 and its low evaporative resistance and high moisture permeability index.

The effects of the application of reflectors in the outer shell and of the incorporation of PCMs in the multilayer system were evaluated through the experimental procedure developed to evaluate the transient behaviour. In the first case, it was concluded that the application of IR reflectors on the outer shell does not have a significant impact on the heating delay and, in addition, it significantly increases the evaporative resistance of the assembly. In the second case, although the incorporation of PCMs is beneficial since it decreases the initial heating rate of the assembly by 79.5 %, it also dramatically delays its cooling by almost 4500 seconds. In addition to this, the incorporation of PCMs in the firefighter jacket also increases its weight and evaporative resistance.

6 Assessment of the work done

6.1 Objectives Achieved

The main objective of this dissertation was the development of a multilayer system with integrated PCMs for a firefighter's jacket and, subsequently, the development of an experimental procedure to evaluate its transient behaviour.

Regarding the development of the multilayer system, firstly the fabrics that would be part of the assembly were selected. Secondly, the effect of applying IR reflectors and incorporating PCM pouches constructed from polymer X was studied. A multi-layer system was developed, consisting of two fabrics and an intermediate layer with PCM pouches, capable of significantly delaying the heating of the assembly.

Concerning the other main objective, an experimental procedure was developed to evaluate the transient behaviour of the solution under study, where it is possible to simulate the different phases of exposure of a firefighter during firefighting (i.e., direct exposure to heat flux followed by a cooling period).

6.2 Limitations and future work

The major limitation of this work consisted in the size of textile samples available. Due to their small size, it was necessary to use the heel area of the thermal manikin foot. For this reason, it was not possible to determine the thermal insulation and evaporative resistance of the assembly, since it was not possible to place a PCM pouch in this zone. Thus, it is suggested to determine these properties of the multilayer system.

Considering that the PCM form has proved to be a determining factor in its performance, it is also suggested to study PCM A in powder form since it is commercialised this way by the supplier. PCM B is not marketed in powder form and, therefore, this study is not suggested.

One of the most important considerations to be taken in the development of protective clothing is mass transfer, as seen in chapter 2.1. Hence, it is recommended to optimise the performance of the developed multilayer system, considering relevant aspects related to mass transfer (e.g., the effect of the distribution/quantity of water inside the jacket on the occurrence of burns)

Finally, it is suggested to develop a firefighter's jacket for structural and proximity fires, where a moisture barrier is included.

6.3 Final Assessment

This dissertation provided me with the opportunity to work with a wide range of new techniques, instruments and methodologies, which enriched my knowledge not only in the area of heat transfer and personal protective equipment, but also in the textile industry.

Besides that, this dissertation allowed me to develop soft skills such as communication and teamwork, since I had the opportunity to work not only with researchers of CeNTI, but also of CITEVE and CEFT.

7 References

[1] C. Hertleer, S. Odhiambo, and L. V. A. N. Langenhove, "Protective clothing for firefighters and rescue workers," 2013, doi: 10.1533/9780857097620.2.338.

[2] R. P. Avsec, "Firefighter PPE goes high performance," 2019. https://www.firerescue1.com/fire-products/turnoutgear/articles/firefighter-ppe-goes-high-performance-hhI1M3nxD5zETJTn/ (accessed Feb. 22, 2021).

[3] "DIF-Jacket." https://difjacketproject.fe.up.pt/ (accessed Apr. 14, 2021).

[4] A. Fonseca, S. F. Neves, and J. B. L. M. Campos, "Thermal performance of a PCM firefighting suit considering transient periods of fire exposure , post – fire exposure and resting phases," *Appl. Therm. Eng.*, vol. 182, no. February 2020, p. 115769, 2021, doi: 10.1016/j.applthermaleng.2020.115769.

[5] NFPA, "Standard on Protective Ensembles for Structural Fire Fighting and Proximity Fire Fighting," 1971.

[6] U. S. A. N. S. R. D. and E. Center, "Wildland Firefighter Personal Protective Equipment (PPE) Selection Guide," no. June, 2014, [Online]. Available: https://www.dhs.gov/sites/default/files/publications/Wild-FF-PPE-SG_0614-508.pdf.

[7] ISO 15831:2004 - Clothing - Physiological effects - Measurement of thermal insulation by means of a thermal manikin.

[8] ASTM F 2370 - 05: Standard Test Method for Measuring the Evaporative Resistance of Clothing Using a Sweating Manikin.

[9] ISO 6942:2002 - Protective clothing — Protection against heat and fire — Method of test: Evaluation of materials and material assemblies when exposed to a source of radiant heat.

[10] G. Song, S. Mandal, and R. M. Rossi, *Thermal Protective Clothing for Firefighters*. Woodhead Publishing, 2017.

[11] S. F. Neves, J. B. L. M. Campos, and T. S. Mayor, "Effects of clothing and fibres properties on the heat and mass transport, for different body heat/sweat releases," *Appl. Therm. Eng.*, 2017, doi: 10.1016/j.applthermaleng.2017.01.074.

[12] A. Morel, G. Bedek, F. Salaün, and D. Dupont, "A review of heat transfer phenomena and the impact of moisture on firefighters' clothing and protection," *Ergonomics*, vol. 57, no. 7, pp. 1078–1089, 2014, doi: 10.1080/00140139.2014.907447.

[13] M. Raimundo, "Personal protective clothing and safety of firefighters near a high intensity fire front," vol. 44, pp. 514–521, 2009, doi: 10.1016/j.firesaf.2008.10.007.

[14] J. R. Lawson, W. D. Walton, N. P. Bryner, F. K. Amon, W. D. Walton, and N. P. Bryner, "Estimates of Thermal Properties for Fire Fighters ' Protective Clothing Materials Estimates of Thermal Properties for Fire Fighters ' Protective Clothing Materials."

[15] G. Song, "Modeling thermal protection outfits for fire exposures," no. January 2002, 2018.

[16] G. Song and F. Wang, *Firefighters ' Clothing and Equipment*, 1st Editio. New York, United States: CRC Press, 2019.

[17] M. A. R. Bhuiyan, L. Wang, A. Shaid, I. Jahan, and R. A. Shanks, "Silica aerogel-integrated nonwoven protective fabrics for chemical and thermal protection and thermophysiological wear comfort," *J. Mater. Sci.*, vol. 55, no. 6, pp. 2405–2418, 2020, doi: 10.1007/s10853-019-04203-2.

[18] A. Di Giovanni, "Demystifying Turnout Gear Terminology," 2009. https://www.fireengineering.com/firefighting/demystifying-turnout-gear-terminology/#gref (accessed Feb. 10, 2021).

[19] R. Paul, *High Performance Technical Textiles*, First Edit. Leeds, United Kingdom: John Wiley & Sons Ltd, 2019.

[20] A. A. Mandot, P. N. Patel, and B. H. Patel, "I Preparation of flame-retardant polymer nanocomposite textiles," no. January 2017, 2016.

[21] X. Zhang and M. Shi, "Flame Retardant Vinylon/Poly(m-phenylene isophthalamide) Blended Fibers with Synergistic Flame Retardancy for Advanced Fireproof Textiles," *J. Hazard. Mater.*, 2018, doi: 10.1016/j.jhazmat.2018.10.091.

[22] J. He, Y. Lu, L. Wang, and N. Ma, "On the Improvement of Thermal Protection for Temperature-Responsive Protective Clothing Incorporated with Shape Memory Alloy," 2018, doi: 10.3390/ma11101932.

[23] E. N. Valendik and I. V. Kosov, "Effect of thermal radiation of forest fire on the environment," *Contemp. Probl. Ecol.*, vol. 1, no. 4, pp. 399–403, 2008, doi: 10.1134/s1995425508040012.

[24] "C&G Flame Resistant And Arc Flash Clothing." http://barbaralundy.co.za/ (accessed May 08, 2021).

[25] L. Jin, P. K. Park, K. A. Hong, and K. J. Yoon, "Effect of aluminized fabrics on radiant protective performance of fire proximity suit materials," *Ann. Occup. Hyg.*, vol. 59, no. 2, pp. 243–252, 2015, doi: 10.1093/annhyg/meu081.

[26] S. Mondal, "Phase change materials for smart textiles – An overview," *Int. J. Heat Mass Transf.*, vol. 28, pp. 1536–1550, 2008, doi: 10.1016/j.applthermaleng.2007.08.009.

[27] L. F. Cabeza, I. Martorell, L. Miró, A. I. Fernández, and C. Barreneche, *Introduction to thermal energy storage (TES) systems*. Woodhead Publishing Limited, 2015.

[28] A. Fonseca, T. S. Mayor, and J. B. L. M. Campos, "Guidelines for the specification of a PCM layer in Firefighting Protective Clothing Ensembles," *Appl. Therm. Eng.*, 2018, doi: 10.1016/j.applthermaleng.2018.01.028.

[29] Microtek laboratories, "Understanding Phase Change Material (PCM)." https://www.microteklabs.com/understanding-pcms?hsCtaTracking=204fb278-0545-4644-8dca-b4f15b6ccb77%7C231dd359-abc0-435a-acd5-b0b425b8f34b (accessed Feb. 19, 2021).

[30] D. Mantz, "How to Determine what Type of Phase Change Material is a Good Fit for your Application," pp. 1–9, 2018.

[31] G. Song and S. Mandal, *Testing and evaluating the thermal comfort of clothing ensembles*. Elsevier Ltd., 2016.

[32] S. Rashidi and M. Samimifar, *Chapter 12114 - Organic Phase Change Materials*. Elsevier Ltd., 2020.

[33] A. R. Hedaoo and A. Hedaoo, "Phase change material review 1," *Int. J. Eng. Res. Gen. Sci.*, vol. 4, no. 2, pp. 203–208, 2016.

[34] Rubitherm, "PCM RT-LINE." https://www.rubitherm.eu/en/index.php/productcategory/organische-pcm-rt (accessed Feb. 15, 2021).

[35] PLUSS, "PCMs Product Range." https://www.pluss.co.in/product-range-PCM.php (accessed Feb. 15, 2021).

[36] CrodaTherm, "Bio-based Phase Change Materials." https://www.crodatherm.com/en-gb (accessed Feb. 15, 2021).

[37] "Making shape memory springs." https://matthey.com/en/products-and-services/medical-components/resource-library/making-shape-memory-springs (accessed Feb. 12, 2021).

[38] A. Greszta, G. Bartkowiak, and A. Dabrowska, "Development of Smart Textile Materials with Shape Memory Alloys for Application in Protective Clothing," 2020, doi: https://doi.org/10.3390/ma13030689.

[39] D. Congalton, "Shape Memory Alloys For Use in Thermally Activated Clothing , Protection Against Flame and Heat," vol. 226, no. February, pp. 223–226, 1999.

[40] N. Ma, Y. Lu, J. He, and H. Dai, "Application of shape memory materials in protective clothing : a review," *J. Text. Inst.*, vol. 0, no. 0, pp. 1–9, 2018, doi: 10.1080/00405000.2018.1532783.

[41] ASTM C1371 - 04a: Standard Test Method for Determination of Emittance of Materials Near Room Temperature Using Portable Emissometers.

[42] F. Wang, "Measurements of clothing evaporative resistance using a sweating thermal manikin: An overview," *Ind. Health*, vol. 55, no. 6, pp. 473–484, 2017, doi: 10.2486/indhealth.2017-0052.

[43] S. P. Athavale, "A Review of various coating methods," p. 53, 2015.

[44] ASTM E 903 - 96: Standard Test Method for Solar Absorptance, Reflectance, and Transmittance of Materials Using Integrating Spheres.

[45] ASTM D 2244 - 05: Standard Practice for Calculation of Color Tolerances and Color Differences from Instrumentally Measured Color Coordinates.

[46] G. Sharma, W. Wu, and E. N. Dalal, "The CIEDE2000 color-difference formula: Implementation notes, supplementary test data, and mathematical observations," *Color Res. Appl.*, vol. 30, no. 1, pp. 21–30, 2005, doi: 10.1002/col.20070.

[47] W. Li, R. Wang, D. Li, and D. Fang, "A model of temperature-dependent Young's modulus for ultrahigh temperature ceramics," *Phys. Res. Int.*, vol. 2011, 2011, doi: 10.1155/2011/791545.

[48] K. Balani, V. Verma, A. Agarwal, and R. Narayan, "Physical, Thermal, and Mechanical Properties of Polymers," *Biosurfaces*, pp. 329–344, 2015, doi: 10.1002/9781118950623.app1.

[49] S. Ahmad, K. Ali, M. Rizwan, and M. Ashraf, "Heat and mass transfer attributes of copper-aluminum oxide hybrid nanoparticles flow through a porous medium," *Case Stud. Therm. Eng.*, vol. 25, no. January, p. 100932, 2021, doi: 10.1016/j.csite.2021.100932.

[50] N. P. Avdelidis, T.-H. Gan, C. Ibarra-Castanedo, and X. P. V. Maldague, "Infrared thermography as a nondestructive tool for materials characterisation and assessment," *Thermosense Therm. Infrared Appl. XXXIII*, vol. 8013, p. 801313, 2011, doi: 10.1117/12.887403.

[51] A. FLIR Systems, *The ultimate infrared handbook for R&D professionals*. FLIR AB, 2012.

Appendix A - Fabrics certifications

The certifications of the fabrics under study are presented in Table A.1.

Table A.1 - Certifications of the fabrics under study

Fabric	Certification	
Outer shell A	Firefighting	EN 469:2005
	Anti-static for explosion risk	EN 1149-5:2008, EN 1149-3:2004
Outer shell B	Industrial flame & heat hazards	EN ISO 11612 A1,A2,B1,C1,E2,F1:2015
	Short-duration thermal exposures from fire	NFPA 2112:2018
	Wildland firefighting	EN 15614:2007
	Anti-Static for explosion risk	EN 1149-5:2018, EN 1149-3:2004
Inner layer A	Firefighting	EN 469:2006/A1
	Industrial flame & heat hazards	EN ISO 11612 A1, A2, B1, C2, F3:2015
Inner layer B	Firefighting	EN 469:2005
Inner layer C	Firefighting	EN 469:2006/A1
Inner layer D	Firefighting	EN 469:2005

Appendix B - Emissometer calibration

The procedure for calibrating the emissometer was as follows:

1. Place the reference standards on the heat sink as shown in Figure 4, with 2-3 drops of water underneath;
2. Place the detector on the high emissivity reference standard (emittance about 0.88) and wait 60-90 seconds for the reading to stabilise. If the read value is not equivalent to the standard's emissivity, the offset must be adjusted.
3. Place the detector on the low emissivity reference standard (emittance about 0.06) and wait 60-90 seconds for the reading to stabilise. If the read value is not equivalent to the standard's emissivity, the offset must be adjusted.

Appendix C - Calculation of IR reflective pigment mass

The calculation of the IR reflective pigment mass is directly related to the desired IR reflective pigment concentration in volume. The IR reflective pigment concentration in volume is calculated using equation C1:

$$\%\ CPV = \frac{V_P}{V_P + V_L} \times 100 \tag{C1}$$

Where *CPV* is the IR reflective pigment concentration in volume in %, V_P is the IR reflective pigment volume in mL and V_L is the binding agent solids volume in mL.

Using the IR reflective pigment volume, it is possible to calculate the IR reflective pigment mass that needs to be measured using equation C2:

$$m_P = V_P \times \rho_P \tag{C2}$$

Where m_P is the IR reflective pigment mass in g, V_P is the IR reflective pigment volume in mL and ρ_P is the IR reflective pigment bulk density in $g \cdot cm^{-3}$.

Appendix D - Evaluation of the IR reflector formulation dispersion

Dispersion is a fundamental step in the production process of a formulation, which aims to separate and disaggregate the pigment particles, eliminating agglomerations. This allows the incorporation of the pigments in the formulation to be homogeneous and, therefore, it is of great importance to assess the quality of the dispersion.

The dispersion is evaluated by dipping a glass rod into the formulation and gently sliding it over a transparent substrate. In Figure D.1 (a) is an example of an incomplete dispersion, where it is possible to see undispersed pigment particles forming scratches surrounded in red. In Figure D.1 (b) is an example of a complete dispersion, where it is not possible to see these scratches of undispersed pigment particles.

(a) (b)

Figure D.1 - Evaluation of formulation dispersion: (a) incomplete dispersion and (b) complete dispersion.

Appendix E - CIEDE2000 system

As stated earlier, the CIEDE2000 system is based on the CIELAB system. Thus, from two CIELAB colour values it is possible to determine the colour difference according to the CIEDE2000 colour-difference formula [46].

The CIELAB colour coordinates *L**, *a** and *b** are determined by the equations E1, E2 and E3, respectively:

$$L^* = 116 \times \left(\frac{Y}{Y_n}\right)^{\frac{1}{3}} - 16 \quad \text{(E1)}$$

$$a^* = 500 \times \left[\left(\frac{X}{X_n}\right)^{\frac{1}{3}} - \left(\frac{Y}{Y_n}\right)^{\frac{1}{3}}\right] \quad \text{(E2)}$$

$$b^* = 200 \times \left[\left(\frac{Y}{Y_n}\right)^{\frac{1}{3}} - \left(\frac{Z}{Z_n}\right)^{\frac{1}{3}}\right] \quad \text{(E3)}$$

Where *X*, *Y* and *Z* are the spectral trichromatic values of the sample and X_n, Y_n and Z_n are the spectral trichromatic values of the reference blank [45].

The CIEDE2000 colour coordinates *L'*, *a'* and *b'* are determined by the equations E4, E5 and E6, respectively:

$$L' = L^* \quad \text{(E4)}$$

$$a' = (1 + G) \times a^* \quad \text{(E5)}$$

$$b' = b^* \quad \text{(E6)}$$

Where *G* is given by equation E7:

$$G = 0.5 \times \left(1 - \sqrt{\frac{\overline{C^*}^7}{\overline{C^*}^7 + 25^7}}\right) \quad \text{(E7)}$$

where $\overline{C^*}$ is the arithmetic mean of the CIELAB *C** values of the sample and standard determined by the equation E8:

$$C^* = \sqrt{(a^*)^2 + (b^*)^2} \quad \text{(E8)}$$

In addition to the colour coordinates, it is also necessary to calculate the specimen or industry dependent parameters K_L, K_C and K_H (default values) and the colour space dependent parameters S_L, S_C, S_H and R_T.

The local tolerance weights S_L, S_C and S_H are determined by the equations E9, E10 and E11, respectively:

$$S_L = 1 + \frac{0.015 \times (\overline{L'} - 50)^2}{\sqrt{20 + (\overline{L'} - 50)^2}} \quad \text{(E9)}$$

$$S_C = 1 + 0.045 \times \overline{C'} \quad \text{(E10)}$$

$$S_H = 1 + 0.045 \times \overline{C'} \times T \quad \text{(E11)}$$

Where T is given by equation E12:

$$T = 1 - 0.17\cos(\overline{h'} - 30°) + 0.24\cos(2\overline{h'}) + 0.32\cos(3\overline{h'} + 6°) - 0.2\cos(4\overline{h'} - 63°) \quad \text{(E12)}$$

And $\overline{h'}$ by equation E13:

$$\overline{h'} = arctan\left(\frac{b'}{a'}\right) \quad \text{(E13)}$$

The R_T term computes a rotation of the colour difference volume in the blue and purple-blue regions of the CIELAB diagram and it is determined by the equation E14:

$$R_T = -\sin(2 \times \Delta\theta) \times R_c \quad \text{(E14)}$$

Where $\Delta\theta$ is determined by the equation E15:

$$\Delta\theta = 30 \times exp\left(-\left[\frac{\overline{h'} - 275°}{25}\right]^2\right) \quad \text{(E15)}$$

And R_c by equation E16:

$$R_C = 2 \times \sqrt{\frac{\overline{C^*}^7}{\overline{C^*}^7 + 25^7}} \quad \text{(E16)}$$

Lastly, the CIEDE2000 colour-difference formula is given by equation E17:

$$\Delta E_{00} = \sqrt{\left(\frac{\Delta L'}{K_L S_L}\right)^2 + \left(\frac{\Delta C'}{K_C S_C}\right)^2 + \left(\frac{\Delta H'}{K_H S_H}\right)^2 + R_T\left(\frac{\Delta C'}{K_C S_C}\right)\left(\frac{\Delta H'}{K_H S_H}\right)} \quad \text{(E17)}$$

Where $\Delta L'$, $\Delta C'$ and $\Delta H'$ are determined by the equations E18, E19 and E20, respectively:

$$\Delta L' = L'_s - L'_r \quad \text{(E18)}$$

$$\Delta C' = C'_s - C'_r \quad \text{(E19)}$$

$$\Delta H' = \frac{a'_r \times b'_s - a'_s \times b'_r}{\sqrt{0.5 \times (C'_r \times C'_s + a'_r \times a'_s + b'_r \times b'_s)}} \quad \text{(E20)}$$

Where *r* refers to the reference and *s* refers to the sample.

Appendix F - Heat flux of IR lamps

The determination of the heat flux of the IR lamps was done using the following procedure:

1. Weigh the copper sample;
2. Adjust the height between the tabletop and the IR lamps;
3. Turn on the IR lamp(s) and allow to stabilize for 10 minutes;
4. Place and fix the data logger on the surface of the copper sample and place them on an extruded polystyrene support as shown in Figure F.1.

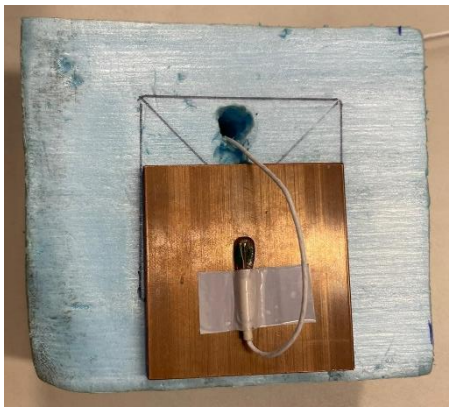

Figure F.1 - Copper sample with the data logger on the extruded polystyrene support.

5. After stabilization of the heat source, start data acquisition (temperature versus time) and place the assembly in the center of the IR lamps installation as shown in Figure F.2;

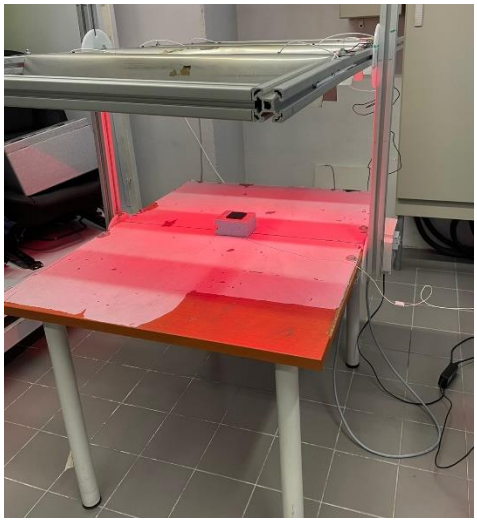

Figure F.2 - Installation for determining the heat flux of IR lamps.

6. Stop data acquisition after ensuring a thermal increment of 12 ºC compared to the starting point.

The copper sample used was painted black in order to have a higher absorbance, thus minimising losses.

The heat flux emitted by IR lamp(s) is then determined from equation F1:

$$Q = \frac{m_c \times c_{p_c} \times R}{A_c \times \alpha_c} \quad \text{(F1)}$$

Where Q is the heat flux emitted by IR lamp(s) in $W \cdot cm^{-2}$, m_c is the mass of the copper sample in g, c_{p_c} is specific heat of the copper sample in $J \cdot g^{-1} \cdot ºC^{-1}$, R is the is the slope of the line of the graph of temperature versus time in the linear zone of thermal increment of 12 ºC in $ºC \cdot s^{-1}$, A_c is area of the copper sample in cm^{-2} and α_c is absorptivity coefficient of the copper sample. All values were determined experimentally, except for the specific heat of the copper where the literature value of 0.385 $J \cdot g^{-1} \cdot ºC^{-1}$ was considered [49].

The heat flux was determined for the central lamp and for all three lamps of the installation for heights of 30, 50 and 80 cm and are presented in Figure F.3.

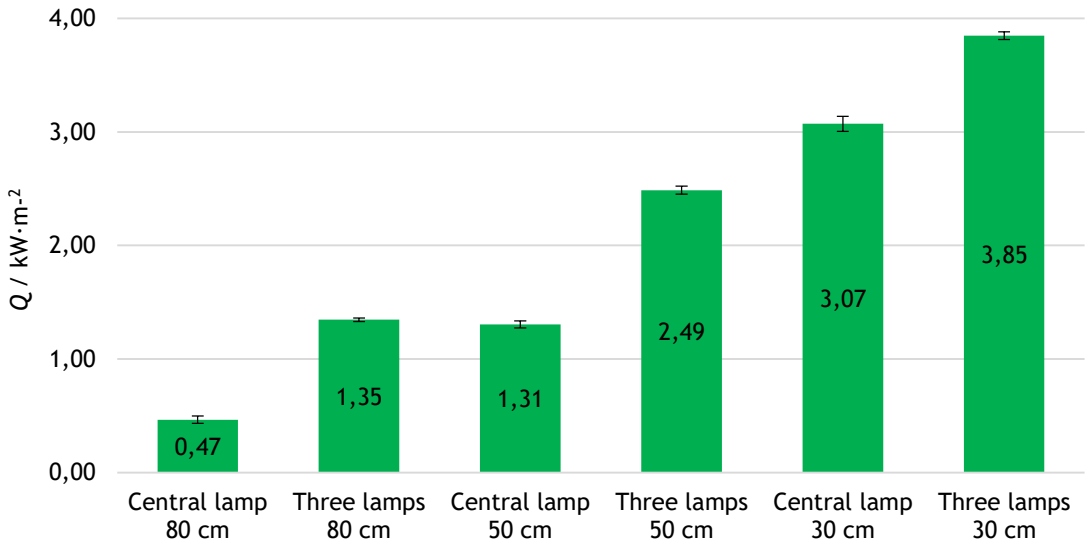

Figure F.3 - Heat fluxes from the installation of IR lamps and the respective standard deviations.

From the analysis of Figure F.3, it can be seen that the highest heat flux is achieved with the three lamps of the installation turned on at a height of 30 cm and has a value of 3.85 $kW \cdot m^{-2}$. As expected, it can also be seen that the lower the height, the lower the influence of the two additional lamps, since less radiation from the side lamps reaches the sample (aligned with the central lamp).

Appendix G - Infrared thermography

Infrared thermography is a non-contact and non-destructive measurement technique based on the detection of radiation in the infrared spectrum that allows the visualisation of the surface temperature [50]. All objects at temperatures above absolute zero emit infrared radiation and the higher the surface temperature of the object, the greater the amount of infrared radiation emitted. The radiated energy measured by a thermographic camera is converted into temperature values using the Stefan-Boltzmann equation:

$$E = \varepsilon \sigma T^4 \quad \text{(G1)}$$

where E is the radiation in $W \cdot m^{-2}$, ε the emissivity, σ the Stefan–Boltzmann constant with value 5.67×10^{-8} $W \cdot m^{-2} \cdot K^{-4}$ and T the surface temperature in K [51].

Appendix H - Stress-strain curves from tensile tests with polymer X

This appendix contains the stress-strain curves of the tensile tests performed on the polymer X strips and pouches.

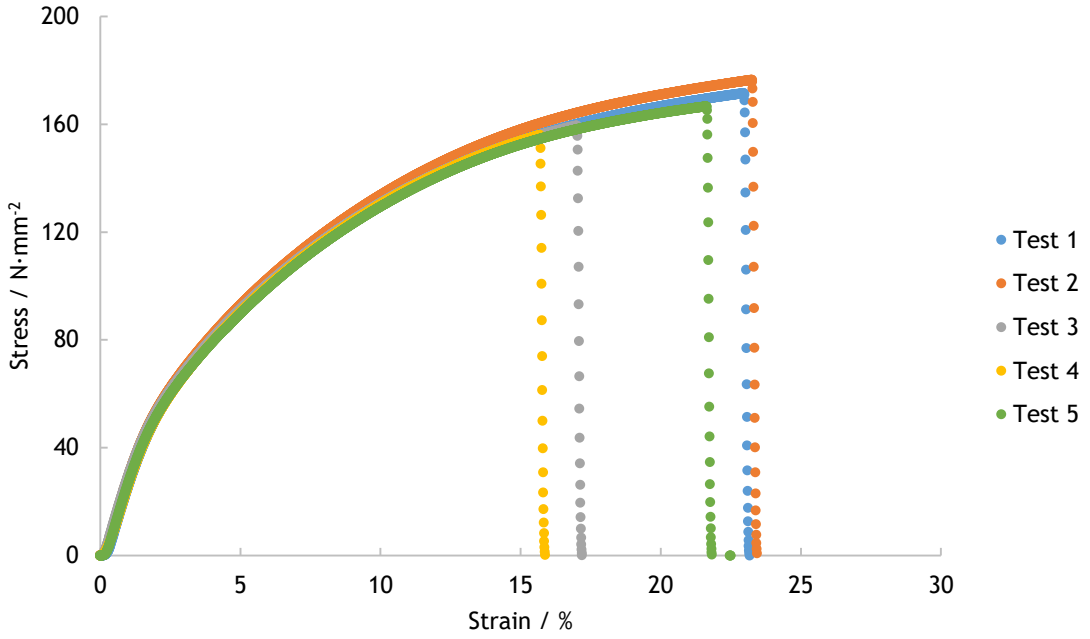

Figure H.1 - Stress-strain curve of strips without heat cycles at $T = T_{room}$.

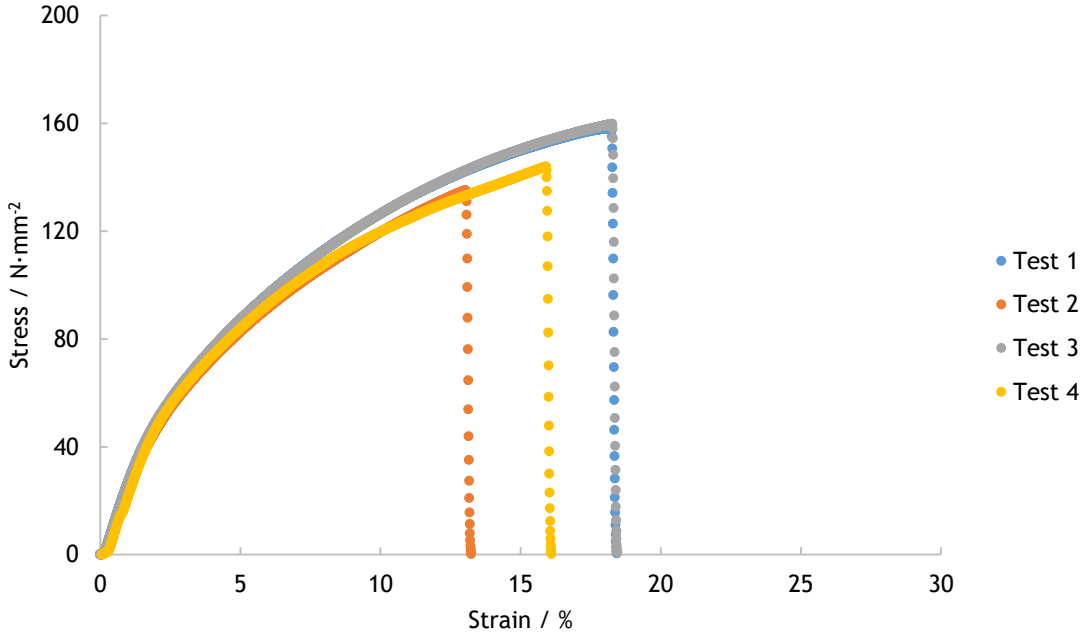

Figure H.2 - Stress-strain curve of strips without heat cycles at T = 50 °C.

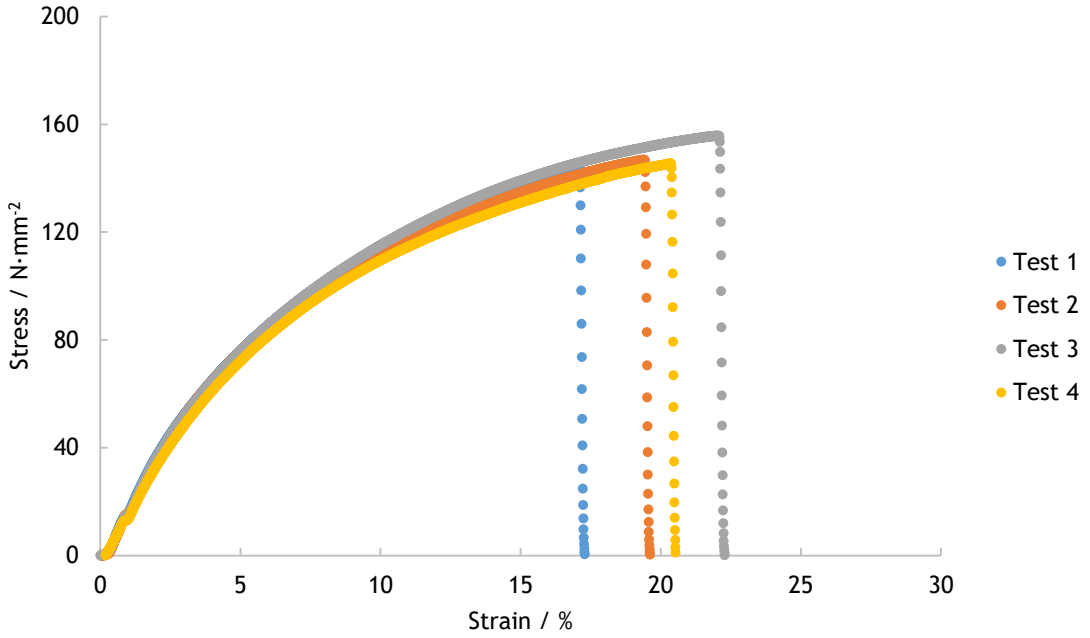

Figure H.3 - Stress-strain curve of strips without heat cycles at T = 80 °C.

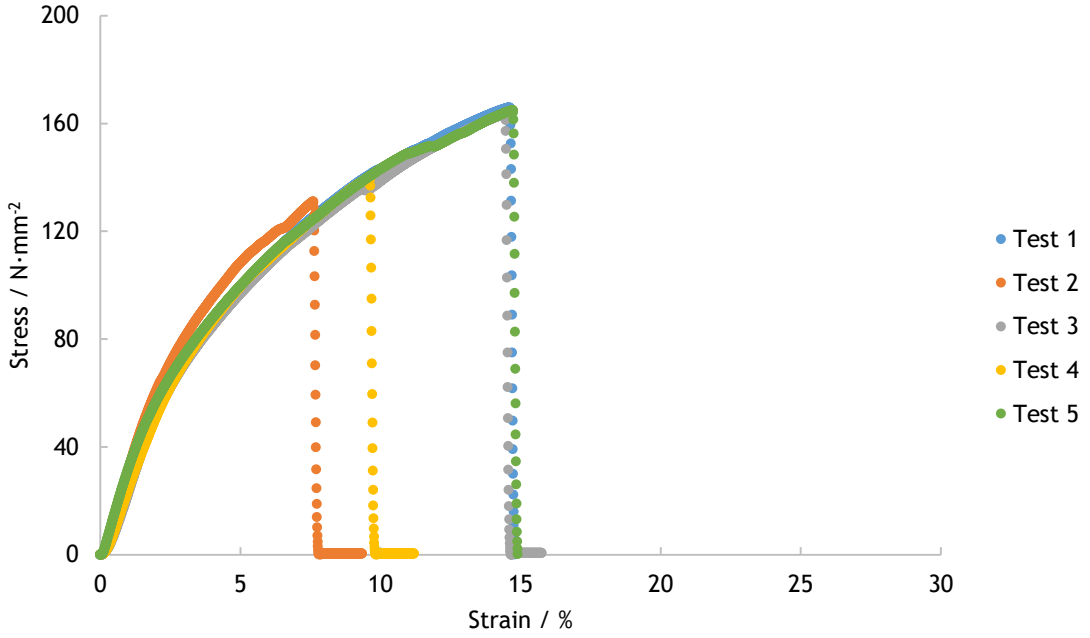

Figure H.4 - Stress-strain curve of pouches constructed manually without heat cycles at $T = T_{room}$.

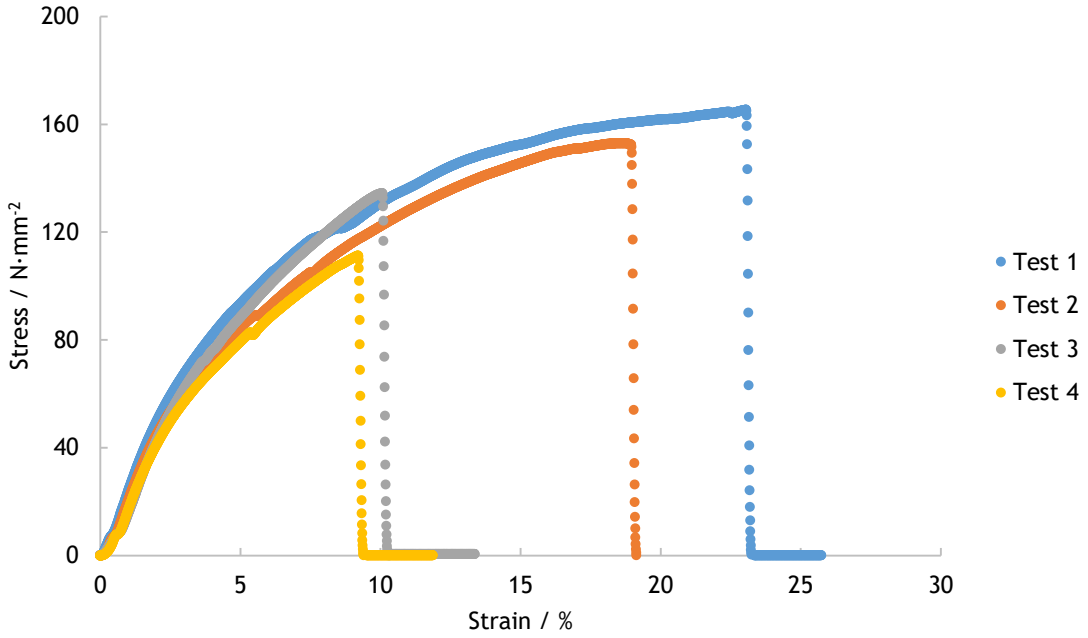

Figure H.5 - Stress-strain curve of pouches constructed manually without heat cycles at T = 50 °C.

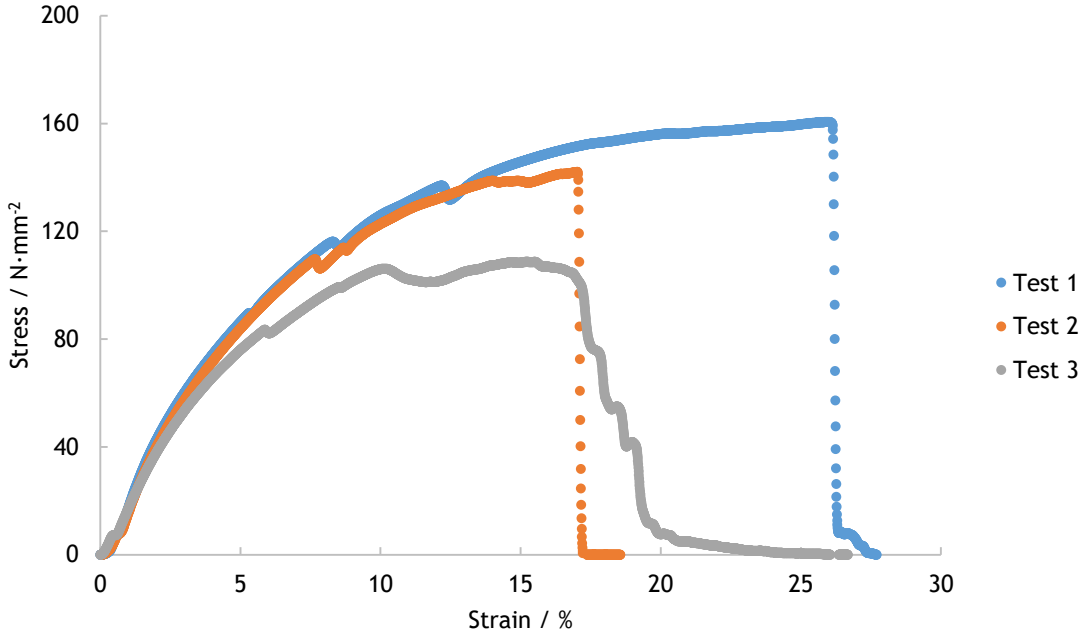

Figure H.6 - Stress-strain curve of pouches constructed manually without heat cycles at T = 80 °C.

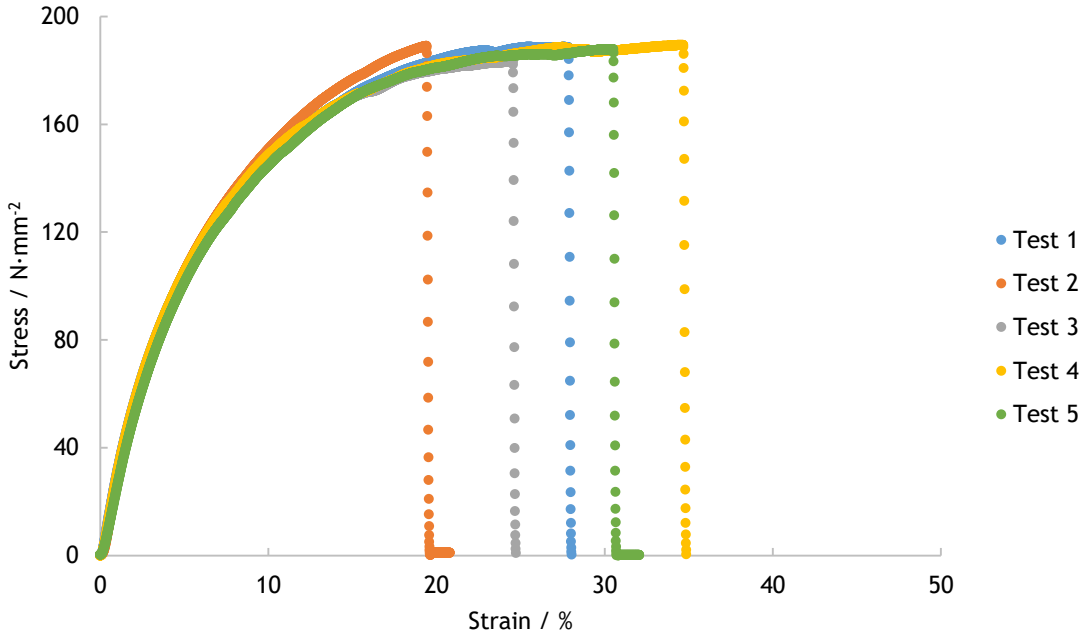

Figure H.7 - Stress-strain curve of pouches constructed manually with heat cycles at $T = T_{room}$.

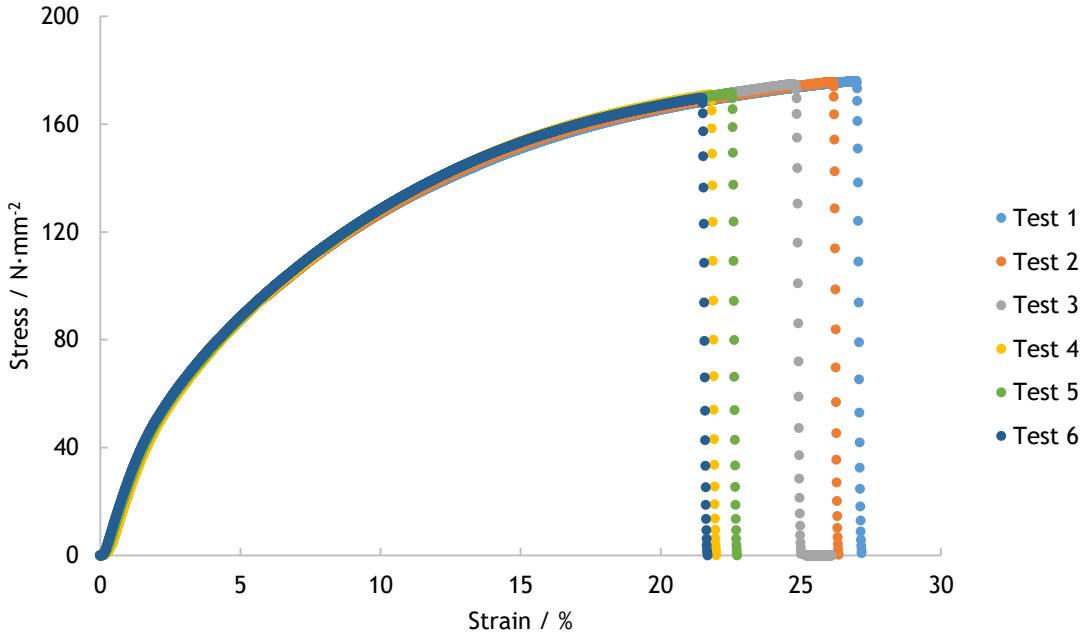

Figure H.8 - Stress-strain curve of pouches constructed by bonding without heat cycles at $T = T_{room}$.

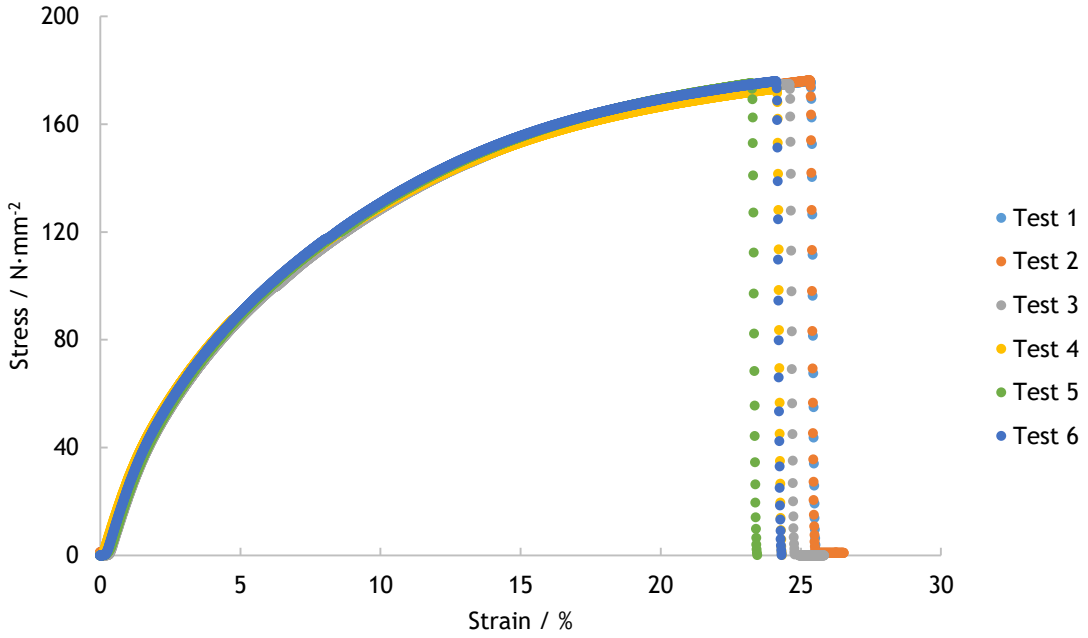

Figure H.9 - Stress-strain curve of pouches constructed by bonding with heat cycles at $T = T_{room}$.

Appendix I - Ambient test conditions for the evaluation of transient behaviour

Table I.1 and Table I.2 show the ambient conditions in the beginning of the tests for the evaluation of the transient behaviour of the PCM pouches and the assemblies, respectively.

Table I.1 - Ambient test conditions for the evaluation of transient behaviour of the PCM pouches

PCM	Geometry	Test	*T* / ºC	*RH* / %
A	Square	1	25.5	59.0
		2	24.1	57.2
	Rectangle	1	24.3	61.0
		2	25.1	54.8
B	Square	1	22.9	59.0
		2	22.8	57.1
	Rectangle	1	24.2	47.2
		2	23.7	59.8
C	Square	1	23.3	57.8
		2	22.5	56.9
	Rectangle	1	22.5	60.3
		2	25.0	61.1

Table I.2 - Ambient test conditions for the evaluation of transient behaviour of the assemblies

Assembly	Test	*T* / ºC	*RH* / %
Outer shell + PCM pouch + Inner layer	1	25.0	60.1
	2	23.5	60.9
Outer shell (functionalised) + PCM pouch + Inner layer	1	25.0	60.2
	2	25.4	56.9
Outer shell + Inner layer	1	25.6	58.1
	2	25.9	58.5

Appendix J - Evaluation of the homogeneity of PCM pouches

The homogeneity of the PCM pouches can be assessed using the thermal camera images. For the treatment of these images, the polymer X emissivity (0.77 ± 0.01) and the environmental conditions of each test present in Appendix I were required. Figure J.1, J.2 and J.3 shows the thermal camera images for the times 0, 4 and 8 minutes for the PCMs A, B and C, respectively, in square and rectangle pouches.

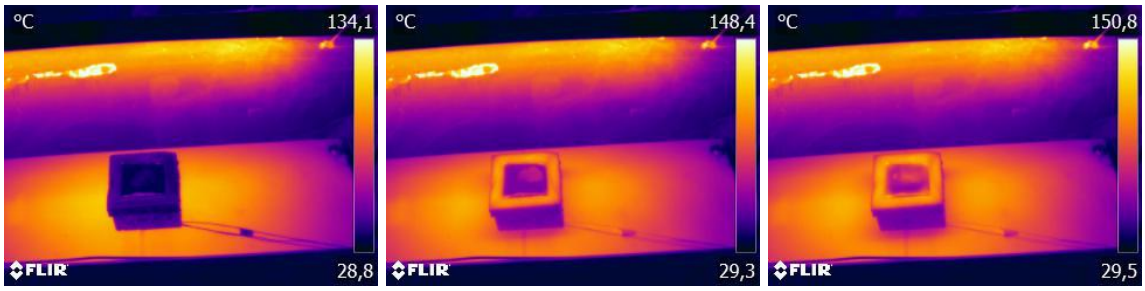

(a) (b) (c)

(d) (e) (f)

Figure J.1 - Thermal camera images of the pouches with PCM A: (a) square at t = 0 min; (b) square at t = 4 min; (c) square at t = 8 min; (d) rectangle at t = 0 min; (e) rectangle at t = 4 min; (f) rectangle at t = 8 min.

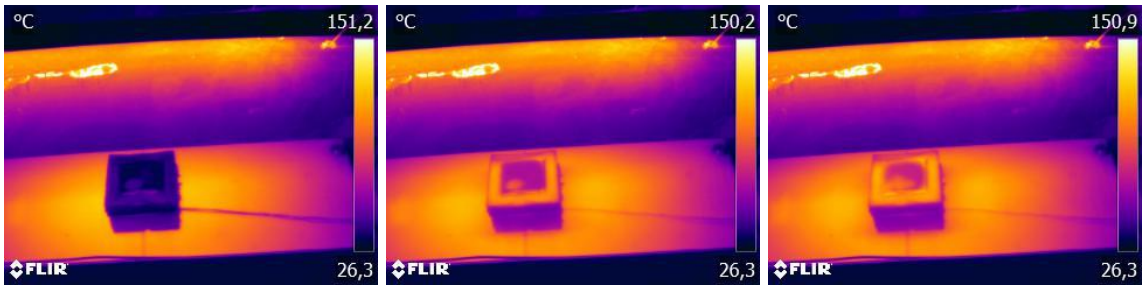

Figure J.2 - Thermal camera images of the pouches with PCM B: (a) square at t = 0 min; (b) square at t = 4 min; (c) square at t = 8 min; (d) rectangle at t = 0 min; (e) rectangle at t = 4 min; (f) rectangle at t = 8 min.

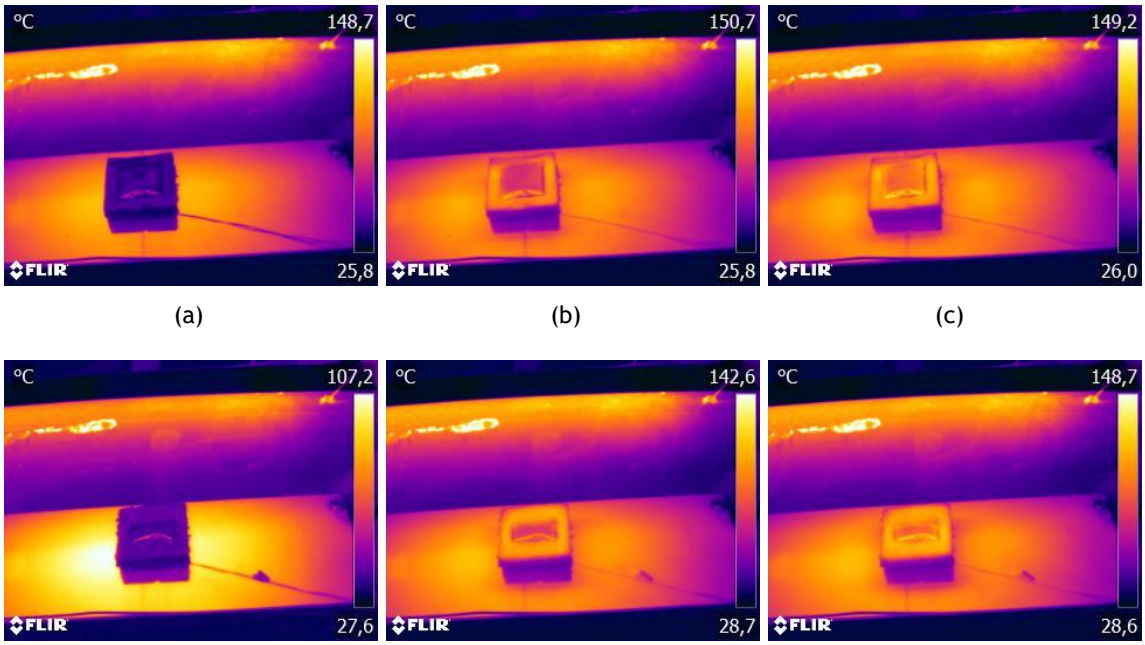

Figure J.3 - Thermal camera images of the pouches with PCM C: (a) square at t = 0 min; (b) square at t = 4 min; (c) square at t = 8 min; (d) rectangle at t = 0 min; (e) rectangle at t = 4 min; (f) rectangle at t = 8 min.